Research Square

Preprints are preliminary reports that have not undergone peer review.
They should not be considered conclusive, used to inform clinical practice,
or referenced by the media as validated information.

Integrated Analysis of Pyroptosis-Energy Metabolism Identifies a Prognostic Immunometabolic Signature in Lung Adenocarcinoma

Kang Luo
Yunnan University
Guangyuan Guo
Yan'an Hospital Affiliated To Kunming Medical University
Haoyu Liu
Affiliated Qujing Hospital of Kunming Medical University
Wenwen Huang
Yan'an Hospital Affiliated To Kunming Medical University
Xiang Gao
First People's Hospital of Yunnan Province
Yunfei Shi
First Affiliated Hospital of Kunming Medical University
Yiming Han
Yan'an Hospital Affiliated To Kunming Medical University
Shen Han
Yan'an Hospital Affiliated To Kunming Medical University
Mingyao Meng
Yan'an Hospital Affiliated To Kunming Medical University
Bingrong Zheng
zhengbr@ynu.edu.cn

Yunnan University

Research Article

Keywords: Lung adenocarcinoma, Pyroptosis, Energy metabolism, Immunometabolism, Prognostic signature, Tumor immune microenvironment

Posted Date: October 28th, 2026

DOI: https://doi.org/10.21203/rs.3.rs-11062352/v1

License: This work is licensed under a Creative Commons Attribution 4.0 International License.
Read Full License

Additional Declarations: No competing interests reported.

Integrated Analysis of Pyroptosis-Energy Metabolism Identifies a Prognostic Immunometabolic Signature in Lung Adenocarcinoma

Kang Luo[1,2,#], Guangyuan Guo[4,#], Haoyu Liu[6,#], Wenwen Huang[7], Xiang Gao[8], Yunfei Shi[2], Yiming Han[4], Shen Han[4,5,*], Mingyao Meng[3,*], Bingrong Zheng[1,*]

[1]School of Medicine, Yunnan University, Kunming 650091, Yunnan, China.
[2]Department of Thoracic Surgery, First Affiliated Hospital of Kunming Medical University, Kunming 650000, Yunnan, China.
[3]Department of Central Laboratory, Yan'an Affiliated Hospital of Kunming Medical University, Kunming 650000, Yunnan, China.
[4]Department of Cardiovascular Surgery, Yan'an Affiliated Hospital of Kunming Medical University, Kunming 650000, Yunnan, China.
[5]Key Laboratory of Cardiovascular Disease of Yunnan Province,Yan'an Affiliated Hospital of Kunming Medical University, Kunming 650000, Yunnan, China.
[6]Affiliated Qujing Hospital of Kunming Medical University, Qujing 655000, Yunnan, China.
[7]Department of Pathology, Yan'an Affiliated Hospital of Kunming Medical University, Kunming 650000, Yunnan, China.
[8]Department of Neurosurgery, The First People's Hospital of Yunnan Province, Kunming 650000, Yunnan, China.

[#]These authors contributed equally to this work. *Corresponding Authors.
Correspondence to:
Professor Shen Han, Department of Cardiovascular Surgery, Yan'an Affiliated Hospital of Kunming Medical University, Kunming 650000, China; Key Laboratory of Cardiovascular Disease of Yunnan Province, Kunming 650000,China. Email: hanshen1140@kmmu.edu.cn

Professor Mingyao Meng, Department of Central Laboratory, Yan'an Affiliated Hospital of Kunming Medical University, Kunming 650000, China. Email: mengmingyao@kmmu.edu.cn

Professor Bingrong Zheng, School of Medicine, Yunnan University, Kunming, Yunnan, 650091, China. Email: zhengbr@ynu.edu.cn

Abstract

Background: Pyroptosis and energy-metabolic reprogramming are closely linked to tumor progression and immune dysfunction, but their integrated relevance in lung adenocarcinoma (LUAD) remains incompletely defined. We aimed to characterize the pyroptosis–energy metabolism (PEM) landscape of LUAD and identify PEM-associated candidate biomarkers.

Methods: TCGA-LUAD and two independent GEO cohorts (GSE31210 and GSE32863) were integrated for transcriptomic analyses. WGCNA, consensus clustering, Cox/LASSO modeling, functional enrichment, regulatory network construction, immune profiling, and gene-level prognostic and diagnostic analyses were performed. Expression of the six signature genes was further assessed by RT–qPCR in 19 paired LUAD and adjacent non-tumor tissues.

Results: Twenty-eight PEM module genes were identified, and consensus clustering defined three molecular subtypes with distinct survival outcomes. A six-gene signature comprising ADORA1, CRTAC1, IL1A, PCSK9, TLR2, and TREM2 significantly stratified overall survival in TCGA-LUAD, with 1-, 3-, and 5-year AUCs of 0.690, 0.649, and 0.627. High-risk tumors showed lower stromal and immune scores, higher tumor purity and tumor mutation burden, and distinct immune-cell infiltration patterns. RT–qPCR showed significantly lower expression of CRTAC1, IL1A, and PCSK9 in tumor tissues, whereas ADORA1, TLR2, and TREM2 did not differ significantly between paired tumor and adjacent non-tumor tissues.

Conclusion: This study identified a six-gene PEM-related signature associated with overall survival and the tumor immune environment in LUAD. CRTAC1 showed the most consistent evidence across transcriptomic datasets, survival analyses, diagnostic evaluation, and paired clinical tissues, with lower expression in tumors and higher expression associated with better survival. These findings support further investigation of CRTAC1 and the other signature genes as biomarkers related to pyroptosis, energy metabolism, and immune regulation in LUAD.

Keywords: Lung adenocarcinoma; Pyroptosis; Energy metabolism; Immunometabolism; Prognostic signature; Tumor immune microenvironment

Introduction

Lung adenocarcinoma (LUAD), the predominant histological subtype of non-small cell lung cancer, remains a major global health burden. Despite advances in screening, molecularly targeted therapy, and immunotherapy, a substantial proportion of patients are diagnosed at advanced stages or eventually develop therapeutic resistance, resulting in limited and often transient clinical benefit. These challenges underscore the need for a deeper understanding of LUAD biology and for robust biomarkers to improve diagnostic and prognostic stratification and inform mechanistic studies[1-4] .

Pyroptosis is a gasdermin-mediated, pro-inflammatory form of programmed cell death with important roles in cancer biology[5]. Inflammasome activation, exemplified by NLRP3 signaling, promotes caspase-dependent gasdermin cleavage and membrane pore formation, facilitating the release of IL-1β, IL-18, and other inflammatory mediators and damage-associated molecular patterns[6,7]. In parallel, metabolic reprogramming supports tumor growth while reshaping antitumor immunity through nutrient competition, lactate accumulation, and adenosine signaling[8,9]. Cellular metabolic states can also influence inflammatory signaling; for example, succinate can promote HIF-1α-dependent IL-1β production, providing a mechanistic link between metabolic remodeling and inflammatory programs[10]. This reciprocal interaction may contribute to an immunologically dysfunctional tumor microenvironment characterized by persistent inflammatory signaling, myeloid enrichment, T-cell dysfunction, and metabolic

restriction[11]. Together, these observations support the concept that pyroptotic signaling and energy metabolism are interconnected determinants of tumor progression and therapeutic response.

Given the complexity and context dependence of this crosstalk, single-cohort or single-layer analyses may be insufficient to capture the full spectrum of pyroptosis–energy metabolism (PEM)-related alterations in LUAD. Integrating independent transcriptomic cohorts with complementary genomic, regulatory, immune, and pharmacological information provides an opportunity to identify reproducible PEM-associated molecular features and to evaluate their clinical relevance across different datasets and analytical platforms[12-14]. Such an approach may facilitate the identification of biologically coherent molecular subtypes, improve prognostic stratification, and uncover regulatory or therapeutic nodes linking inflammatory cell death with tumor metabolism[15,16].

In this study, we integrated multi-cohort transcriptomic and multi-layer molecular data to characterize the pyroptosis–energy metabolism (PEM) landscape of LUAD. In contrast to analyses focused primarily on pyroptosis-related genes, our approach integrated pyroptotic signaling with energy-metabolism-associated transcriptional programs within a unified PEM framework. We identified PEM-related co-expression modules and molecular subtypes, developed a six-gene immunometabolic signature comprising ADORA1, CRTAC1, IL1A, PCSK9, TLR2, and TREM2, and evaluated its prognostic and immune associations. We further constructed regulatory and drug-connectivity networks and assessed expression of the six signature genes by RT–qPCR in paired LUAD and adjacent non-tumor tissues. These analyses identified candidate biomarkers and biological associations for further investigation in LUAD.

Methods

Data acquisition

TCGA-LUAD RNA-seq data (539 tumors and 59 adjacent non-tumor samples), somatic mutation data, and copy-number data were obtained from the NCI Genomic Data Commons under project ID TCGA-LUAD using TCGAbiolinks[17]. Matched clinical data were retrieved from the TCGA Lung Adenocarcinoma (LUAD) cohort in UCSC Xena. For clinicopathological summaries, GDC primary-tumor records were collapsed by the 12-character TCGA patient barcode, yielding 517 unique patients (Supplementary Table S11). Tumor mutational burden (TMB) data were obtained from the cBioPortal Lung Adenocarcinoma (TCGA, PanCancer Atlas) study (study ID: luad_tcga_pan_can_atlas_2018), and TIDE scores were computed using the TIDE framework[18]. TCGA VarScan-derived MAF files were analyzed using maftools[19], while CNV data were analyzed using GISTIC 2.0[20].

Independent transcriptomic datasets included GSE31210 (Affymetrix GPL570; 226 LUAD and 20 normal samples) and GSE32863 (Illumina GPL6884; 58 LUAD and 58 matched normal samples), which were downloaded from GEO and mapped according to platform annotation[21,22]. GeneCards was queried to retrieve 308 pyroptosis-related and 2,507 energy-metabolism-related protein-coding genes (relevance score > 0.5), their intersection, after removal of genes absent across the TCGA/GEO platforms, yielded 90 PEM-related genes (Supplementary Table S2)[23].

Computation of PEM-related phenotype scores (TCGA cohort)

TCGA RNA-seq data were transformed to FPKM/TPM as appropriate, whereas GEO microarrays were normalized independently using platform-specific procedures; absolute expression intensities were not directly compared across platforms. Preprocessing diagnostics are

shown in Supplementary Figure S1. In TCGA-LUAD, single-sample GSEA (ssGSEA), implemented in GSVA, was used to calculate a PEMRG score for each sample[14]. Normal versus LUAD differences were tested by Wilcoxon rank-sum test, and LUAD cases were median-dichotomized for downstream analyses. Clinicopathological distributions between the high- and low-PEMRGs-score groups were summarized descriptively using stacked bar plots.

Weighted gene co-expression network analysis (WGCNA)

WGCNA was performed on the top 25% of the most variable TCGA-LUAD mRNAs using a soft-threshold power of 5. Topological overlap-based clustering with dynamic tree cutting identified modules (minimum size = 100), which were merged at a cut height of 0.2[24]. Module–trait correlations were calculated for tissue type (normal versus LUAD), and PEMRGs intersecting trait-associated modules were retained as PEM module genes.

Molecular subtype identification in TCGA-LUAD

ConsensusClusterPlus was applied to PEM module genes using k = 2–8, 50 resamplings, 80% item subsampling, k-means clustering, and Euclidean distance[25]. The optimal number of clusters was determined from the CDF and delta-area plots. Subtype differences were assessed by Kruskal–Wallis tests, with pairwise Wilcoxon tests and Benjamini–Hochberg correction where appropriate. Subtype-specific survival comparisons were restricted to 526 patients; 13 of the 539 clustered cases were excluded because their OS data did not satisfy the completeness criteria applied to this analysis.

Expression differences in the 28 PEM module genes between LUAD and normal tissues were evaluated separately in TCGA-LUAD, GSE31210, and GSE32863 using Wilcoxon rank-sum tests. Genes with nominal $p < 0.05$ in all three cohorts were considered robust PEM module genes.

Construction of the PEMRGs prognostic model

PEM module genes were first screened by univariable Cox regression ($p < 0.10$). The selected genes were subsequently analyzed using LASSO-Cox with glmnet (family = “cox”, 10-fold cross-validation, 1,000 iterations)[15]. All 11 genes retained by LASSO were then entered into multivariable Cox regression, from which the reported six-gene prognostic model comprising ADORA1, CRTAC1, IL1A, PCSK9, TLR2, and TREM2 was derived. The multivariable six-gene model and RiskScore-based survival analyses were conducted in the model-specific complete-case analysis set (n = 526).

RiskScore = $\Sigma(\beta_i \times \text{expression}_i)$, where β_i is the multivariable Cox coefficient. Patients were median-dichotomized into high- and low-risk groups, and risk distribution, survival status/time, and model-gene expression were visualized.

Differential expression between risk groups was analyzed with limma[26]. DEGs were defined as $|\log_2 FC| > 1$ and adjusted $p < 0.05$ (Benjamini–Hochberg), and visualized by volcano plots.

Functional enrichment (GO) and pathway analysis (KEGG)

GO and KEGG enrichment analyses of prognosis-associated PEMRGs were performed with clusterProfiler[27,28]. GO analyses covered BP, MF, and CC domains; significance was defined as adjusted $p < 0.05$ and FDR $q < 0.05$.

Gene set enrichment analysis (GSEA) and gene set variation analysis (GSVA)

For GSEA, all TCGA-LUAD genes were preranked by $\log_2 FC$ (high versus low risk) and analyzed with clusterProfiler using MSigDB c2.all.v2022.1.Hs.symbols.gmt (seed = 2022; 1,000 permutations; minGSSize = 10; maxGSSize = 500)[29,30]. Adjusted $p < 0.05$ and FDR $q < 0.05$ were considered significant.

GSVA was performed using the C2 curated gene set collection from MSigDB release 2022.1.Hs, retrieved using the msigdbr R package. The C2 collection includes both chemical and genetic perturbation (CGP) and canonical pathway (CP) gene sets. Differential gene sets were defined as adjusted $p < 0.05$ and $|\log_2 FC| > 0.50$.

Protein–protein interaction (PPI) network

A protein-protein interaction network for ADORA1, CRTAC1, IL1A, PCSK9, TLR2, and TREM2 was constructed using STRING v11 for Homo sapiens (NCBI taxonomy ID: 9606) at the highest-confidence interaction threshold (score ≥ 0.900) and was subsequently visualized using Cytoscape v3.9.1[31,32]. Functional similarity among the genes was quantified with GOSemSim[33].

Regulatory and therapeutic interaction networks (mRNA–miRNA, mRNA–TF, mRNA–drug)

For mRNA–miRNA analysis, miRDB predictions (Target Score > 80)[34] were intersected with ENCORI/starBase[35]. mRNA–TF relationships supported by both ChIPBase v3.0 and hTFtarget were retained[36,37], while CTD chemical–gene associations were used to construct a hypothesis-generating mRNA–drug network[38]. Networks were visualized in Cytoscape v3.9.1.

Immune evaluation and correlation analyses

ESTIMATE was used to infer stromal/immune content and tumor purity from TCGA-LUAD expression profiles[39]. TIDE scores were used as computational estimates of immune evasion and predicted response to immune checkpoint blockade[40], whereas TMB data were obtained from the cBioPortal Lung Adenocarcinoma (TCGA, PanCancer Atlas) study (study ID: luad_tcga_pan_can_atlas_2018)[18]. Differences between high- and low-risk groups were assessed using Wilcoxon rank-sum tests, and associations with RiskScore were evaluated using Spearman correlation.

Immune-cell infiltration by ssGSEA

Immune-cell infiltration was quantified using ssGSEA implemented in the GSVA package with predefined immune-cell gene signatures[41,42]. Differences in immune-cell enrichment scores between high- and low-risk groups were assessed using Wilcoxon rank-sum tests. Spearman correlation analyses were performed to evaluate relationships among immune-cell subsets and between immune-cell infiltration and the six signature genes.

Prognostic and diagnostic evaluation of the six signature genes

To further characterize the clinical associations of the six signature genes, gene-level prognostic and diagnostic analyses were performed. For gene-level survival analyses, a separate analysis-specific complete-case set (n = 530) was used, and patients were dichotomized into high- and low-expression groups according to the median expression of each gene. Univariable Cox proportional hazards regression was performed with the low-expression group as the reference, and hazard ratios (HRs) with 95% confidence intervals (CIs) were estimated. Kaplan–Meier curves and two-sided log-rank tests were used to compare overall survival between the two expression groups. Diagnostic performance for distinguishing LUAD tumors from adjacent non-tumor tissues in TCGA-LUAD was assessed by receiver operating characteristic (ROC) analysis, and the area under the curve (AUC) with 95% CI was calculated for each gene.

Quantitative real-time PCR validation in LUAD surgical specimens

Tumor and matched adjacent lung tissues were obtained from 19 patients with histopathologically confirmed primary LUAD undergoing curative-intent resection at the First Affiliated Hospital of Kunming Medical University. Patients who had received neoadjuvant therapy, had another malignancy, or had inadequate tissue or RNA quality were excluded.

Baseline characteristics are provided in Supplementary Table S18. The study protocol was approved by the Ethics Committee of the First Affiliated Hospital of Kunming Medical University (Approval No. (2026) Ethics Review L No. 14) and was conducted in accordance with the Declaration of Helsinki and applicable institutional guidelines and regulations. Written informed consent was obtained from all participants before sample collection.

Total RNA was extracted from fresh-frozen tissues and reverse-transcribed to cDNA. qPCR was performed using SYBR Green with ACTB as the reference gene; reaction mixtures, cycling conditions, primer sequences, and raw data are provided in Supplementary Tables S13–S17. Technical triplicates were averaged at the ΔCt level for each patient and tissue. Normalized log2 expression was expressed as $-\Delta Ct$, and paired tumor-to-adjacent changes were calculated as $\log2(\text{Tumor/Adjacent}) = -\Delta\Delta Ct$. Paired differences were assessed using two-sided Wilcoxon signed-rank tests on patient-level mean ΔCt values, with Benjamini–Hochberg correction across the six genes; FDR $q < 0.05$ was considered significant.

Statistical analysis

Analyses were performed in R 4.1.2. Continuous variables were compared using Student's t-test or the Wilcoxon rank-sum test as appropriate; comparisons among three or more independent groups were performed using Kruskal–Wallis tests unless otherwise specified. Survival distributions were estimated using Kaplan–Meier analysis and compared using log-rank tests; correlations were assessed using Spearman's rho. Benjamini–Hochberg correction was applied for multiple testing where indicated. All P values were two-sided. Complete-case eligibility was defined separately for each survival analysis according to the data requirements of that analysis; consequently, the subtype, multivariable-model, and gene-level analyses included different numbers of patients.

Results

Study workflow

TCGA and GEO cohorts were integrated to characterize the LUAD pyroptosis–energy metabolism (PEM) landscape. The workflow comprised PEMRGs scoring, WGCNA, consensus clustering, prognostic modeling, differential/pathway analyses, immune profiling, regulatory-network construction, and RT–qPCR validation of the six signature genes (Figure 1).

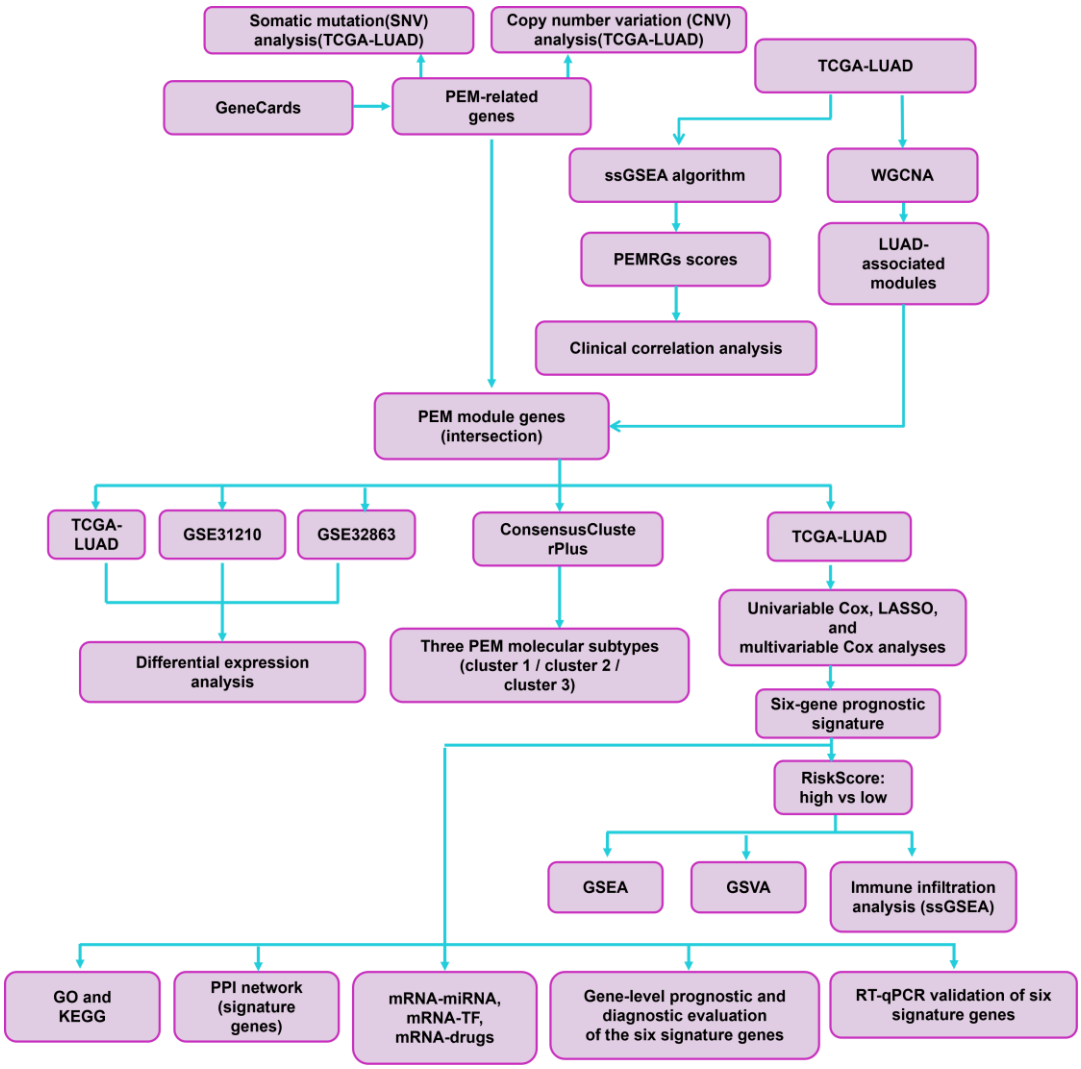


Fig. 1 Overall study workflow. TCGA-LUAD was used as the primary cohort to characterize PEM-related features, including SNV/CNV alterations, ssGSEA-based PEMRG scoring, WGCNA, consensus clustering, and prognostic modeling. Differential expression analyses were performed across TCGA-LUAD, GSE31210, and GSE32863. A six-gene prognostic signature was derived using univariable Cox, LASSO-Cox, and multivariable Cox analyses. Downstream analyses included GSEA, GSVA, GO/KEGG enrichment, immune-cell infiltration, PPI, and mRNA–miRNA, mRNA–TF, and mRNA–drug networks. The six signature genes were further evaluated for prognostic and diagnostic performance and assessed by RT–qPCR in paired LUAD and adjacent non-tumor tissues. Abbreviations: TCGA, The Cancer Genome Atlas; LUAD, lung adenocarcinoma; PEM, pyroptosis–energy metabolism; PEMRGs, pyroptosis- and energy-metabolism-related genes; SNV, single-nucleotide variant; CNV, copy-number variation; ssGSEA, single-sample gene set enrichment analysis; WGCNA, weighted gene co-expression network analysis; LASSO, least absolute shrinkage and selection operator; GSEA, gene set enrichment analysis; GSVA, gene set variation analysis; GO, Gene Ontology; KEGG, Kyoto Encyclopedia of Genes and Genomes; PPI, protein–protein interaction; TF, transcription factor; RT–qPCR, reverse-transcription quantitative polymerase chain reaction.

Mutation analysis of PEMRGs in LUAD patients

After dataset-specific preprocessing, expression distributions for TCGA-LUAD (539 tumors, 59 adjacent non-tumor samples), GSE31210 (226 tumors, 20 normal samples), and GSE32863 (58 tumors, 58 matched normal samples) were examined (Supplementary Figure S1a–f).

Among the 90 PEMRGs in TCGA-LUAD, missense mutations predominated. Most alterations were SNVs, mainly C > A, C > T, and C > G. TP53 was the most frequently mutated gene, followed by NLRP3 and TLR4, and co-mutation patterns were observed (Figure 2a–c).

GISTIC 2.0 revealed widespread CNV alterations, including gains in DHX9, ADORA1, and IKBKE and losses in TP53, YWHAE, and HMGB1 (Figure 2d).

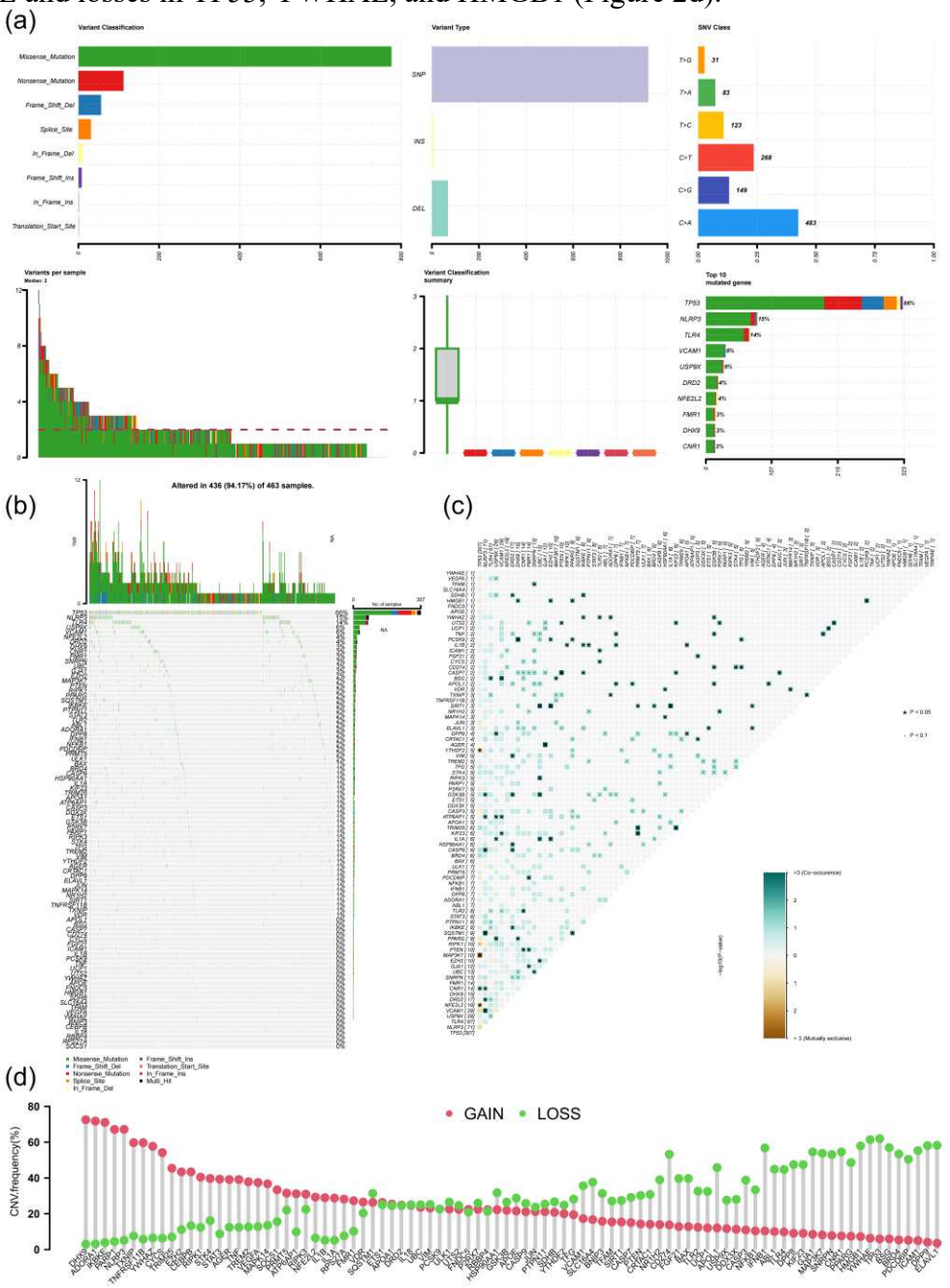


Fig. 2 Somatic alteration landscape of PEM-related genes (PEMRGs) in TCGA-LUAD. (a) maftools summary plots showing variant classification, variant type, single-nucleotide variant (SNV) class, variants per sample, and the top 10 mutated PEMRGs. (b) Oncoplot of mutations across PEMRGs in individual LUAD samples, highlighting TP53, NLRP3, TLR4, VCAM1, USP9X, NFE2L2, DRD2, DHX9, CNR1, and FMR1. (c) Co-mutation heatmap depicting pairwise co-occurrence or mutual exclusivity among PEMRGs. (d) Copy-number variation (CNV) frequencies of PEMRGs, showing recurrent gains (e.g., DHX9, ADORA1, IKBKE) and losses (e.g., TP53, YWHAE, HMGB1). Abbreviations: PEMRGs, pyroptosis- and energy-metabolism-related genes; LUAD, lung adenocarcinoma; SNV, single-nucleotide variant; CNV, copy-number variation.

Construction of PEMRGs scores and clinical associations

The PEMRG score was significantly lower in LUAD than in normal tissues ($P < 0.001$; Figure 3a) and showed high diagnostic discrimination (AUC = 0.919; Figure 3b). LUAD cases were then divided into high- and low-score groups using the median PEMRG score. Descriptive differences in the distributions of T stage, age, sex, and PFI event were observed between the high- and low-PEMRG-score groups, whereas the distributions of N stage, M stage, pathologic stage, OS event, and DSS event were broadly similar (Figure 3c–k).

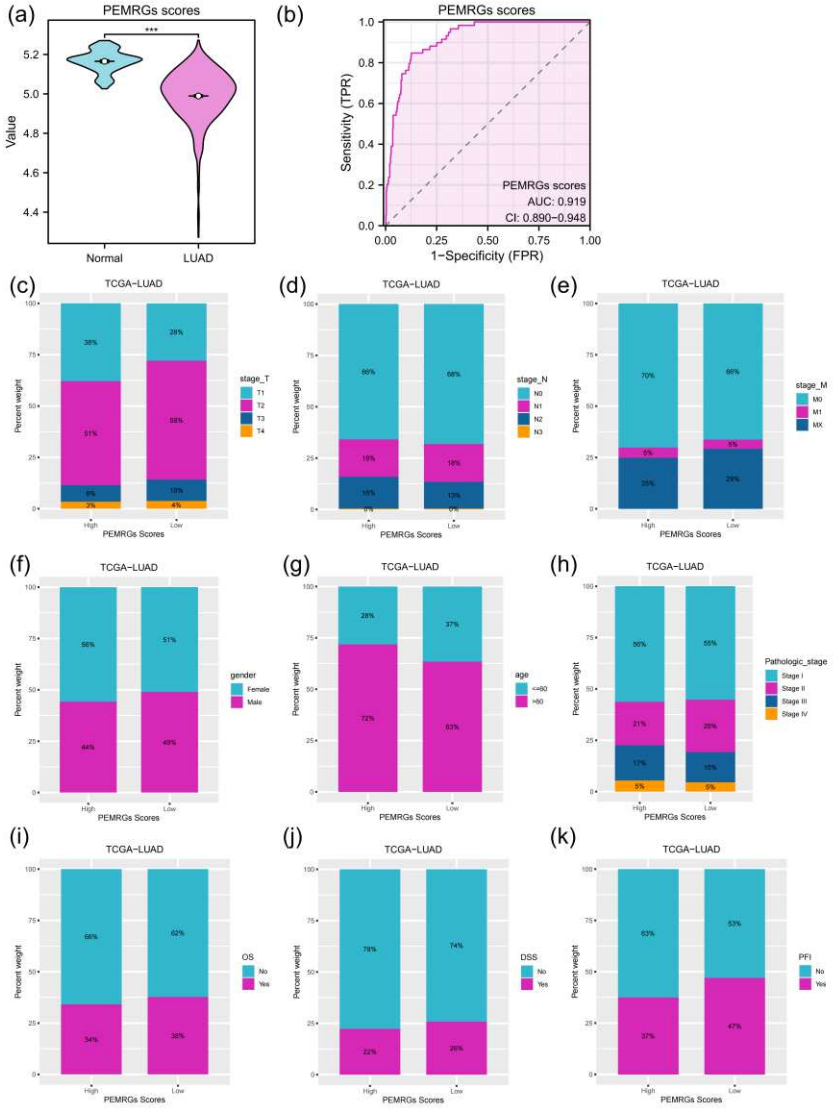


Fig. 3 Construction of PEMRGs scores and clinical associations in TCGA-LUAD.(a) Comparison of the PEMRG score between normal and LUAD tissues (Wilcoxon rank-sum test; ***$p < 0.001$). (b) ROC curve assessing the diagnostic performance of the PEMRG score. (c–k) Stacked bar plots showing distributions of T stage (c), N stage (d), M stage (e), sex (f), age (g), pathologic stage (h), OS event (i), DSS event (j), and PFI event (k) across high- and low-PEMRG-score groups. Abbreviations: PEMRGs, pyroptosis- and energy-metabolism-related genes; ROC, receiver operating characteristic; AUC, area under the curve; OS, overall survival; DSS, disease-specific survival; PFI, progression-free interval.

Identification of co-expression modules by WGCNA

WGCNA identified eight co-expression modules at a soft-threshold power of 5, with the grey set representing unassigned genes (Figure 4a–c). Five modules (MEblue, MEbrown, MEgreen, MEpink, and MEyellow) showed significant associations with tissue type (normal versus LUAD; Figure 4d).

Intersecting these modules with PEMRGs yielded 28 PEM module genes for downstream analyses (Figure 4e–i).

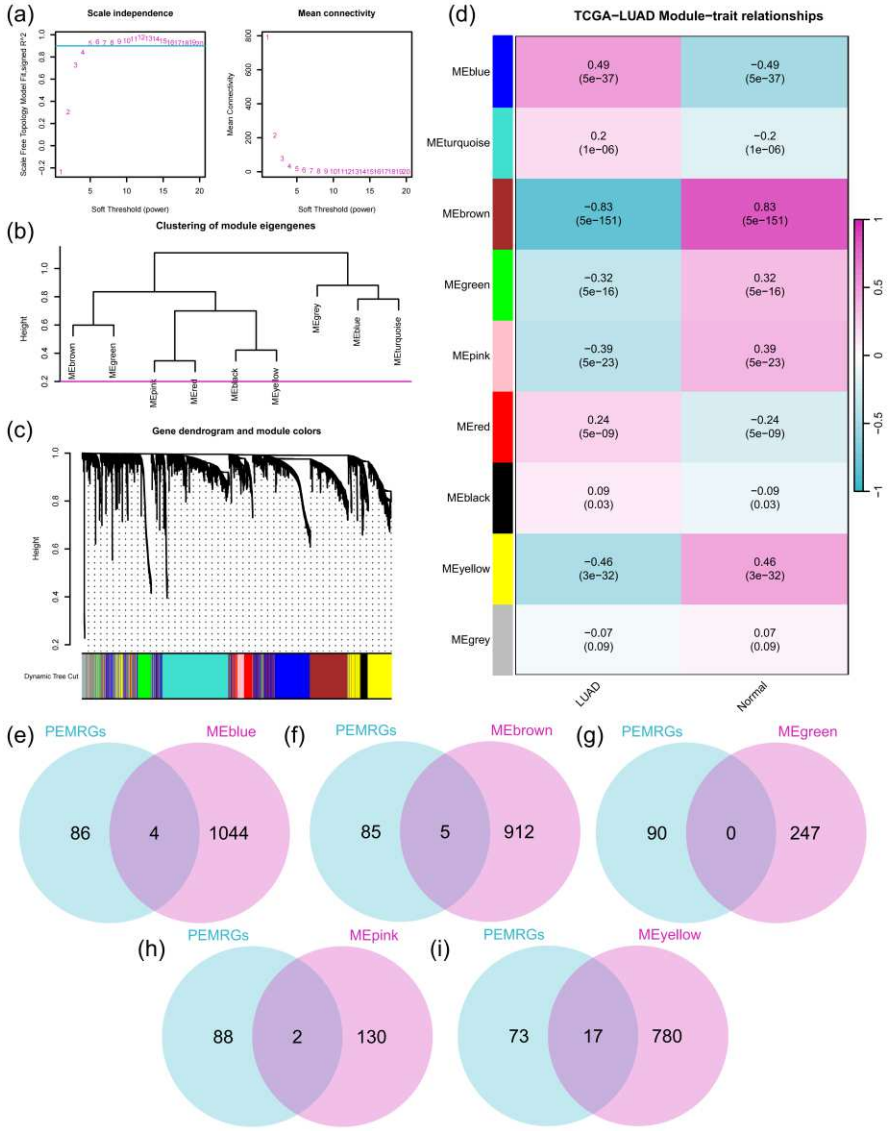


Fig. 4 WGCNA of TCGA-LUAD transcriptome and identification of PEM-related modules. (a) Scale-free topology fit index and mean connectivity across soft-thresholding powers, with β = 5 selected as the optimal power. (b) Clustering dendrogram of module eigengenes. (c) Gene dendrogram with color-coded modules obtained by dynamic tree cutting and subsequent merging. (d) Heatmap of correlations between module eigengenes and tissue type (LUAD versus normal). (e–i) Venn diagrams showing intersections between predefined PEMRGs and genes in the MEblue, MEbrown, MEgreen, MEpink, and MEyellow modules, respectively. Abbreviations: WGCNA, weighted gene co-expression network analysis; TCGA, The Cancer Genome Atlas; LUAD, lung adenocarcinoma; PEMRGs, pyroptosis- and energy-metabolism-related genes.

Construction of LUAD-related molecular subtypes

Consensus clustering of the 28 PEM module genes identified three LUAD subtypes: cluster 1 (n = 145), cluster 2 (n = 179), and cluster 3 (n = 215). CDF and delta-area analyses supported k = 3, with separation among clusters in PCA and distinct subtype-specific expression patterns (Figure 5a–e).

Subtype-specific survival analysis included 526 patients meeting the analysis-specific completeness criteria (cluster 1, n = 143; cluster 2, n = 174; cluster 3, n = 209); 13 of the 539 clustered patients were excluded because their OS data did not satisfy the completeness criteria applied to this analysis. Overall survival differed among the three subtypes (log-rank P = 0.04; Figure 5f), and most PEM module genes varied significantly across clusters, except CEBPB and GJA1 (Figure 5g).

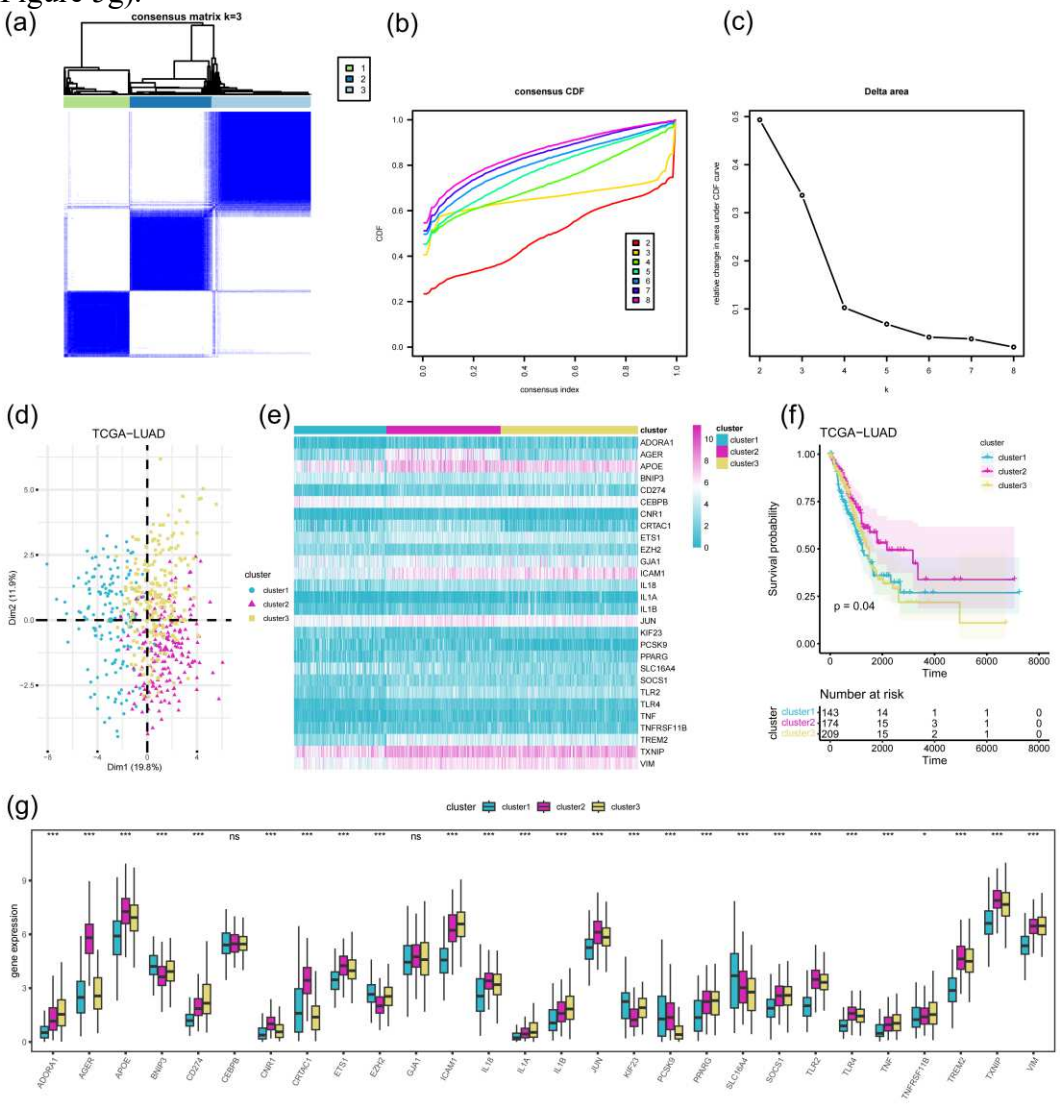


Fig. 5 Consensus clustering of PEM module genes and definition of LUAD molecular subtypes in TCGA-LUAD. (a) Consensus matrix heatmap for k = 3 showing clustering into three PEM-related subtypes (clusters 1–3). (b) Cumulative distribution function (CDF) curves for consensus clustering across different k values. (c) Delta-area plot supporting k = 3 as the selected cluster number. (d) Principal component analysis (PCA) of the 28 PEM module genes illustrating separation among the three clusters. (e) Heatmap showing subtype-specific expression patterns of the 28 PEM module genes across clusters 1–3. (f) Kaplan–Meier overall survival curves comparing the three molecular subtypes among the 526 patients included in the subtype-specific survival analysis (cluster 1, n = 143; cluster 2, n = 174; cluster 3, n = 209). (g) Boxplots of each PEM module gene across the three clusters, with significance indicated (*$p < 0.05$, **$p < 0.01$, ***$p < 0.001$; ns, not significant).

Differential expression of PEM module genes across cohorts

Cross-cohort tumor-versus-normal comparisons identified 19 robust PEM module genes significant in all three datasets: AGER, BNIP3, CD274, CEBPB, CNR1, CRTAC1, ETS1, EZH2, GJA1, IL1A, IL1B, KIF23, PCSK9, PPARG, TLR2, TLR4, TNF, TXNIP, and VIM (Figure 6a). PCSK9 was lower in LUAD in TCGA-LUAD and GSE32863 but higher in GSE31210.

Chromosomal distribution and inter-gene correlations of robust PEM module genes

The 19 robust genes mapped to chromosomes 1, 2, 3, 4, 6, 7, 9, 10, 11, 15, and 20, with chromosome 6 containing the most genes (n = 4; Figure 6b). Correlations were predominantly positive, while BNIP3, EZH2, and KIF23 more often showed negative associations (Figure 6c). Representative correlations were EZH2–KIF23 (r = 0.78), AGER–CRTAC1 (r = 0.69), ETS1–TLR4 (r = 0.68), KIF23–TXNIP (r = −0.55), KIF23–TLR2 (r = −0.53), and CRTAC1–EZH2 (r = −0.51), all $p < 2.2 \times 10^{-16}$ (Figure 6d).

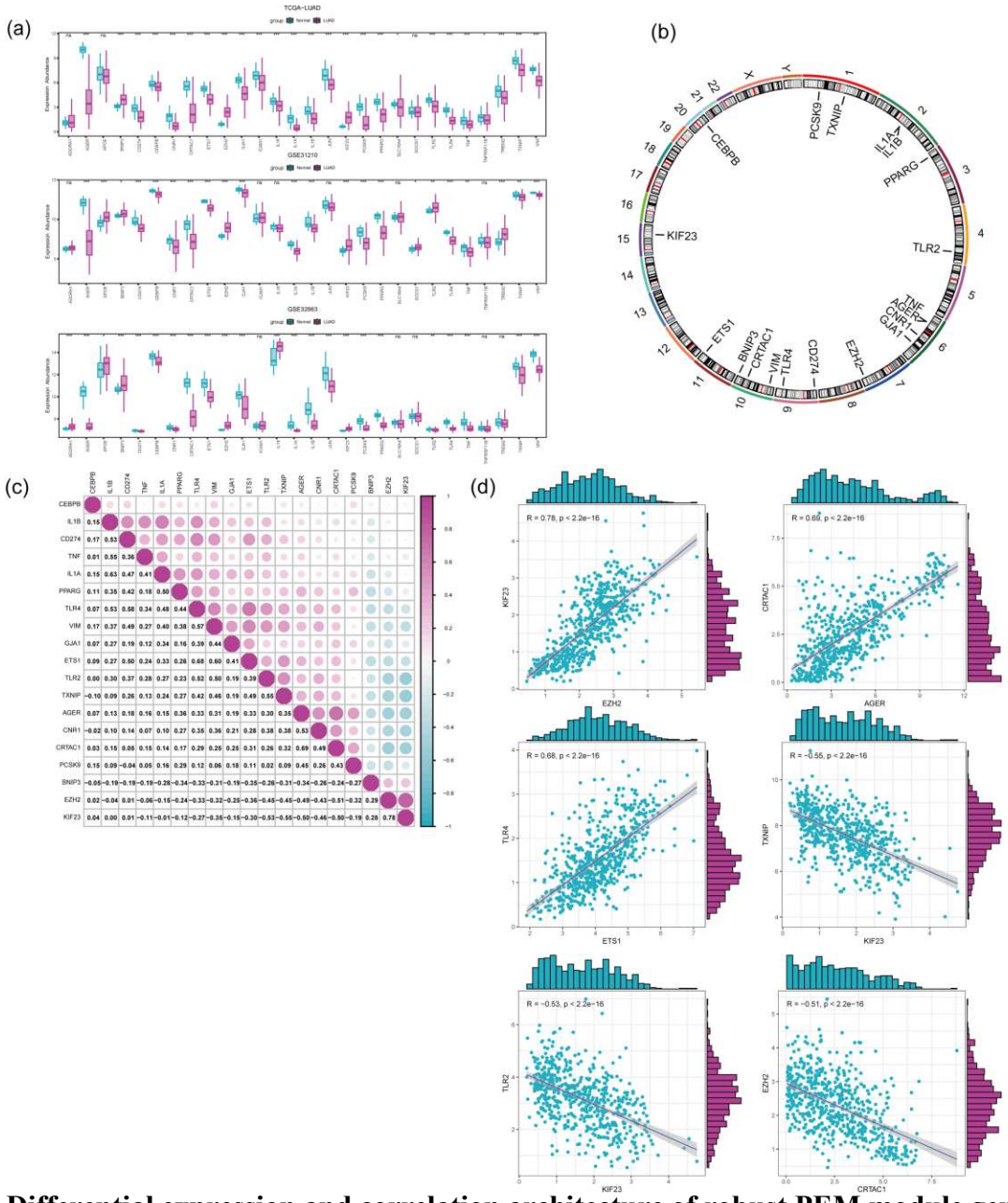


Fig. 6 Differential expression and correlation architecture of robust PEM module genes across cohorts. (a) Expression comparisons of the 28 PEM module genes between normal and LUAD tissues in TCGA-LUAD, GSE31210, and GSE32863 using Wilcoxon rank-sum tests (ns, $P \geq 0.05$; *$p < 0.05$; **$p < 0.01$; ***$p < 0.001$). (b) Chromosomal distribution of the 19 robust PEM module genes that were significantly different between LUAD and normal tissues across all three cohorts (RCircos). (c) Spearman correlation matrix of the 19 robust genes in TCGA-LUAD. (d) Representative correlations for three positively correlated gene pairs (EZH2-KIF23, AGER-CRTAC1, ETS1-TLR4) and three negatively correlated pairs (KIF23-TXNIP, KIF23-TLR2, CRTAC1-EZH2). Abbreviations: TCGA, The Cancer Genome Atlas; LUAD, lung adenocarcinoma; PEM, pyroptosis-energy metabolism.

Construction of the PEMRGs prognostic model and differences between risk groups

Univariable Cox analysis identified 11 prognosis-associated PEM module genes (Supplementary Table S3), all of which were retained by LASSO-Cox (Figure 7a–b). These 11 genes were subsequently entered into multivariable Cox regression, yielding the reported six-gene model comprising ADORA1, CRTAC1, IL1A, PCSK9, TLR2, and TREM2 (Supplementary Table S4): RiskScore = 0.197 × ADORA1 − 0.124 × CRTAC1 + 0.255 × IL1A + 0.199 × PCSK9 − 0.170 × TLR2 − 0.100 × TREM2.

Model construction and RiskScore-based survival analyses were performed in the model-specific complete-case analysis set (n = 526). Overall survival differed significantly between the high- and low-RiskScore groups (log-rank P < 0.001), with 1-, 3-, and 5-year AUCs of 0.690, 0.649, and 0.627, respectively (Figure 7c–f). Comparison of the two risk groups identified 591 DEGs (252 upregulated and 339 downregulated; Figure 7g). The six signature genes showed distinct expression patterns between risk groups (Figure 7h), and RiskScore correlated positively with ADORA1, IL1A, and PCSK9 and negatively with CRTAC1, TLR2, and TREM2 (Figure 7i).

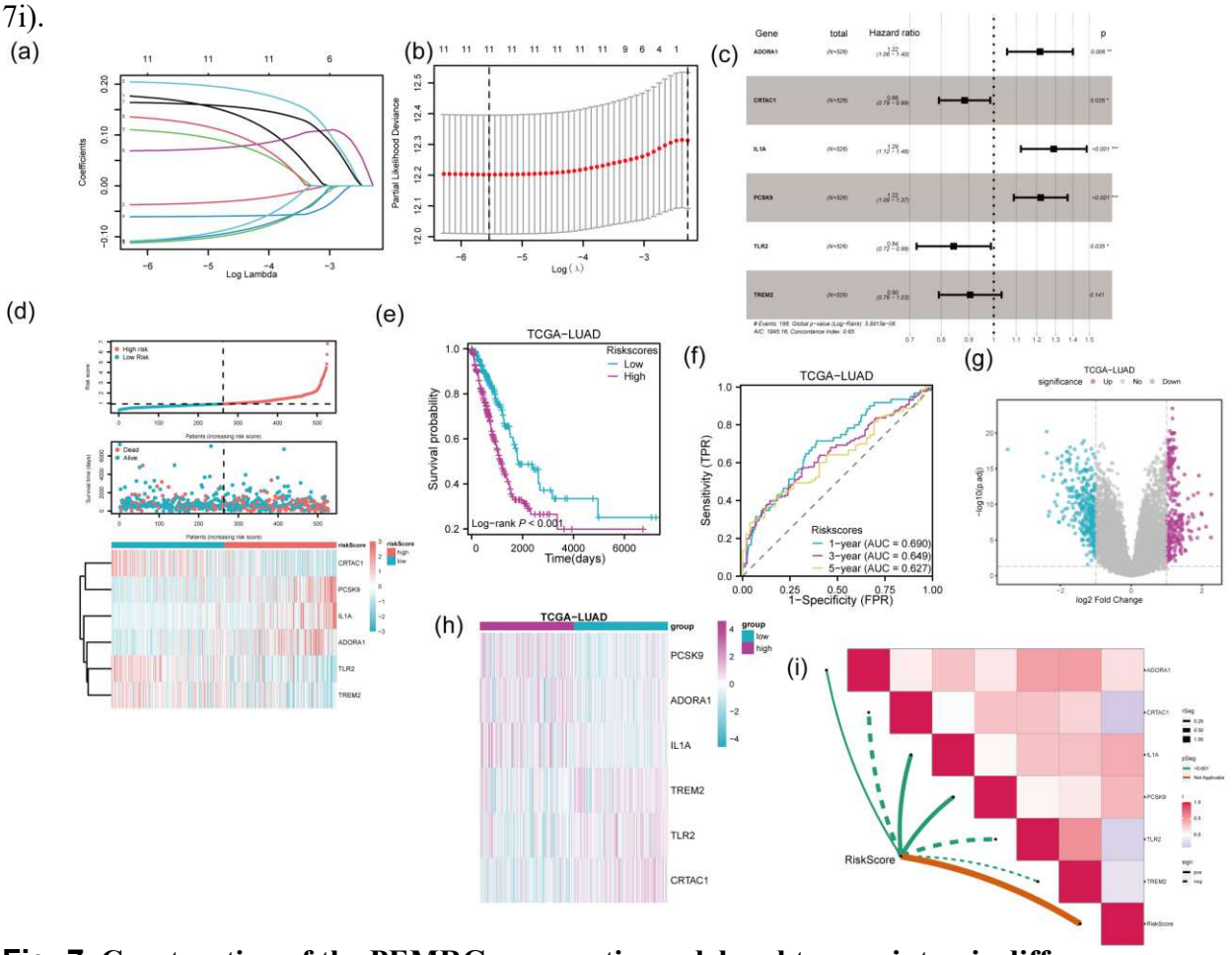


Fig. 7 Construction of the PEMRG prognostic model and transcriptomic differences between risk groups in TCGA-LUAD. (a) LASSO coefficient profiles of candidate PEM-related genes across log(λ) values. (b) Ten-fold cross-validation for selection of the optimal λ in the LASSO-Cox model. (c) Forest plot of the multivariable Cox regression model showing adjusted hazard ratios (HRs) and 95% confidence intervals for the six model genes (ADORA1, CRTAC1, IL1A, PCSK9, TLR2, and TREM2). (d) Risk plot showing RiskScore distribution (top), survival status and follow-up time (middle), and expression of the six genes (bottom),

ordered by increasing RiskScore. (e) Kaplan–Meier overall survival curves for high- versus low-RiskScore groups. (f) Time-dependent ROC curves for 1-, 3-, and 5-year survival based on RiskScore. (g) Volcano plot of differentially expressed genes between high- and low-RiskScore groups. (h) Heatmap showing expression patterns of the six model genes in the two risk groups. (i) Correlation diagram showing Spearman associations between RiskScore and each signature gene, with edge properties indicating correlation sign, magnitude, and statistical significance. Model construction and survival evaluation were based on the model-specific complete-case analysis set (n = 526).

Functional and pathway enrichment of prognosis-associated PEMRGs

GO enrichment of the six prognosis-associated PEMRGs highlighted hypoxia response, secretion, TNF production, leukocyte migration, phagocytosis, pyroptosis, and lipid/ligand-binding functions (Figure 8a; Supplementary Table S5). KEGG analysis identified inflammatory bowel disease, Leishmaniasis, rheumatoid arthritis, osteoclast differentiation, measles, and tuberculosis (Figure 8b; Supplementary Table S5).

GSEA and GSVA analyses between high- and low-RiskScore groups

GSEA identified differential enrichment of Cell Cycle Checkpoints, Glucose Metabolism, Metabolism of Polyamines, Chemokine Signaling, Lipid Metabolism in Senescent Cells, and Leishmania Infection between risk groups (Figure 8C; Supplementary Table S6).

GSVA identified six significantly different pathways, including REACTOME_G2_M_DNA_REPLICATION_CHECKPOINT, CROSBY_E2F4_TARGETS, MONTERO_THYROID_CANCER_POOR_SURVIVAL_UP, LY_AGING_MIDDLE_DN, FINETTI_BREAST_CANCER_KINOME_RED, and REACTOME_PHOSPHORYLATION_OF_EMI1 (Figure 8D–E; Supplementary Table S7).

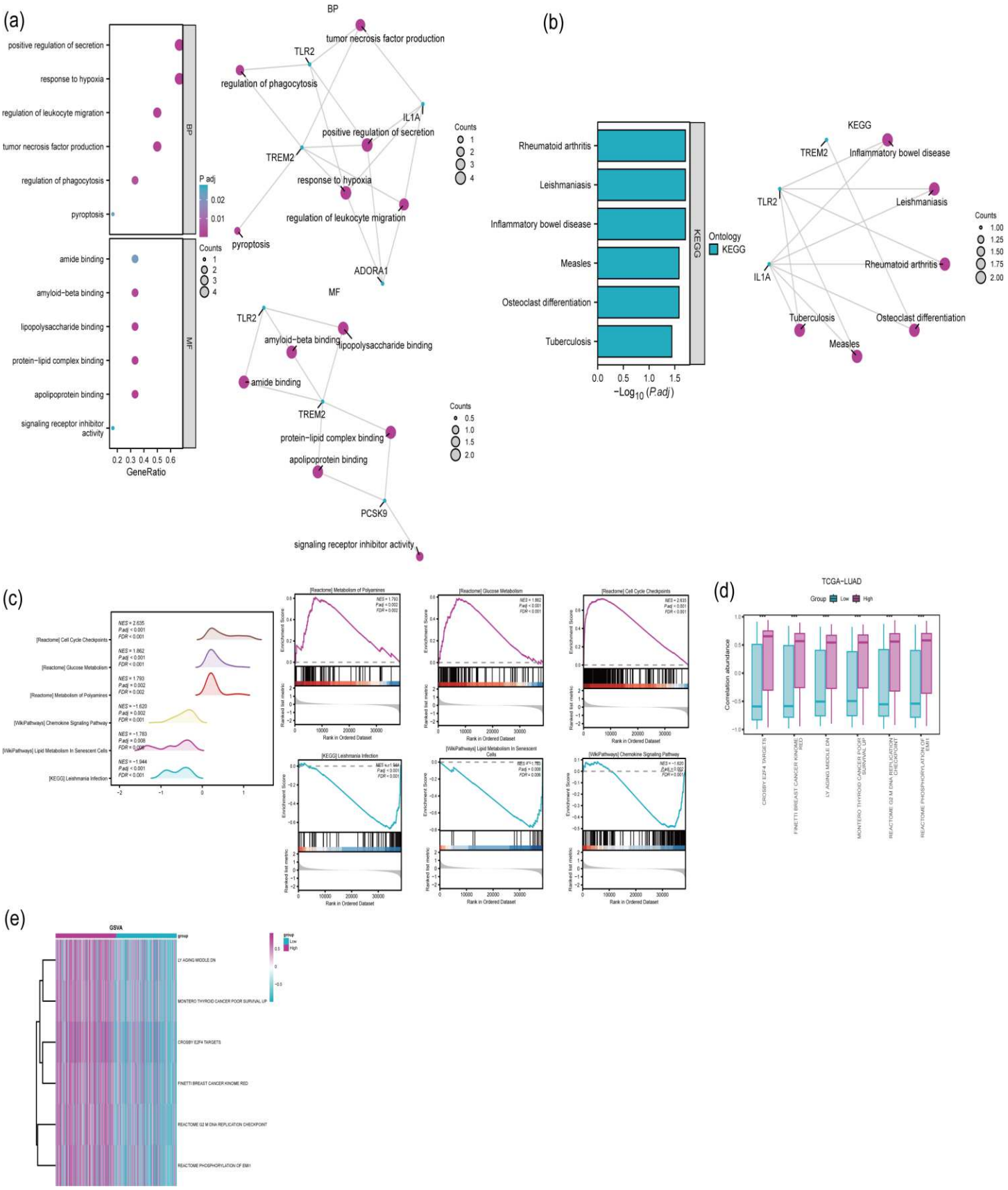

(a)
positive regulation of secretion
response to hypoxia
regulation of leukocyte migration
tumor necrosis factor production
regulation of phagocytosis
pyroptosis
BP
amide binding
amyloid−beta binding
lipopolysaccharide binding
protein−lipid complex binding
apolipoprotein binding
signaling receptor inhibitor activity
MF
P adj
0.02
0.01
Counts
1
2
3
4
0.2 0.3 0.4 0.5 0.6
GeneRatio
BP
tumor necrosis factor production
TLR2
regulation of phagocytosis
IL1A
positive regulation of secretion
TREM2
response to hypoxia
regulation of leukocyte migration
pyroptosis
ADORA1
MF
TLR2
amyloid−beta binding
lipopolysaccharide binding
amide binding
TREM2
protein−lipid complex binding
apolipoprotein binding
PCSK9
signaling receptor inhibitor activity
Counts
0.5
1.0
1.5
2.0
(b)
Rheumatoid arthritis
Leishmaniasis
Inflammatory bowel disease
Measles
Osteoclast differentiation
Tuberculosis
KEGG
Ontology
KEGG
0.0 0.5 1.0 1.5
−Log10 (P.adj)
KEGG
TREM2
Inflammatory bowel disease
TLR2
Leishmaniasis
IL1A
Rheumatoid arthritis
Tuberculosis
Osteoclast differentiation
Measles
Counts
1.00
1.25
1.50
1.75
2.00
(c)
[Reactome] Cell Cycle Checkpoints
[Reactome] Glucose Metabolism
[Reactome] Metabolism of Polyamines
[WikiPathways] Chemokine Signaling Pathway
[WikiPathways] Lipid Metabolism In Senescent Cells
[KEGG] Leishmania Infection
Enrichment Score
Ranked list metric
Rank in Ordered Dataset
(d)
TCGA−LUAD
Group
Low
High
Correlation abundance
CROSBY E2F4 TARGETS
FINETTI BREAST CANCER KINOME RED
LY AGING MIDDLE DN
MONTERO THYROID CANCER POOR SURVIVAL UP
REACTOME G2 M DNA REPLICATION CHECKPOINT
REACTOME PHOSPHORYLATION OF EMI1
(e)
GSVA
group
Low
High
LY AGING MIDDLE DN
MONTERO THYROID CANCER POOR SURVIVAL UP
CROSBY E2F4 TARGETS
FINETTI BREAST CANCER KINOME RED
REACTOME G2 M DNA REPLICATION CHECKPOINT
REACTOME PHOSPHORYLATION OF EMI1

Fig. 8 Functional and pathway enrichment analyses associated with the PEMRGs prognostic signature. (a) GO enrichment analysis of the six prognosis-associated PEMRGs, including a bubble plot and gene-term network views for biological process and molecular function categories. (b) KEGG enrichment analysis showing significantly enriched pathways and corresponding gene-pathway relationships. (c) GSEA results comparing the high- and low-RiskScore groups, presented as a ridge plot and representative enrichment curves for selected pathways. (d) GSVA-based comparison of pathway enrichment scores between high- and low-RiskScore groups. (e) Heatmap showing GSVA enrichment patterns across TCGA-LUAD samples. Abbreviations: GO, Gene Ontology; BP, biological process; MF, molecular function; KEGG, Kyoto Encyclopedia of Genes and Genomes; GSEA, gene set enrichment analysis; GSVA, gene set variation analysis; TCGA, The Cancer Genome Atlas; LUAD, lung adenocarcinoma.

Construction of the PPI network and mRNA–miRNA, mRNA–TF, and mRNA–drug interaction networks

A STRING network constructed at the highest-confidence threshold summarized protein associations among the six signature genes, and GOSemSim analysis indicated the greatest functional relatedness for TLR2 (Figure 9a–b). We identified 55 mRNA–miRNA pairs involving five genes (Figure 9c; Supplementary Table S8), 34 TFs linked to four genes (Figure 9d; Supplementary Table S9), and 46 CTD-associated candidate compounds linked to five genes (Figure 9e; Supplementary Table S10).

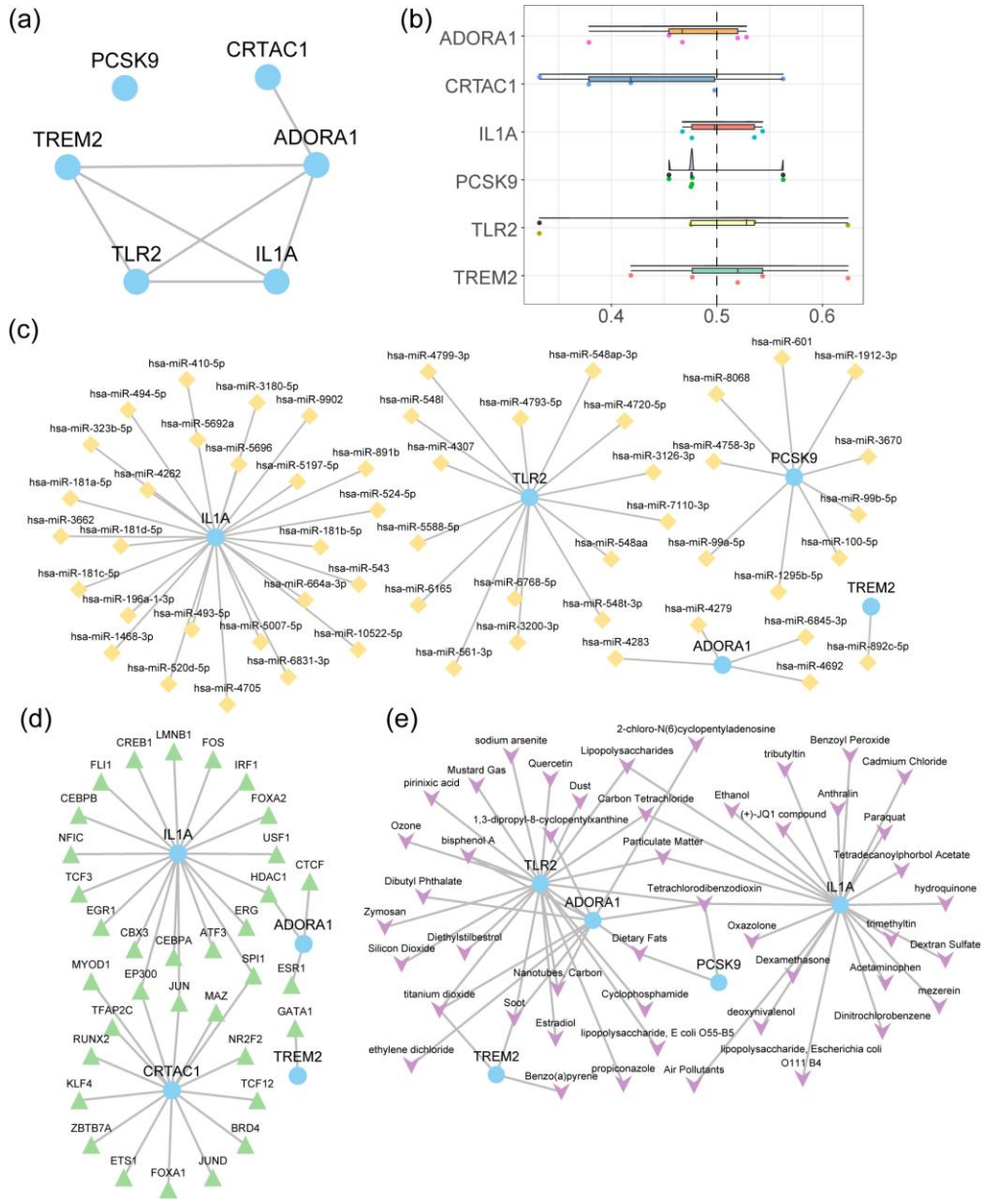


Fig. 9 Interaction and regulatory networks of the six signature genes. (a) Highest-confidence STRING protein-protein interaction (PPI) network of ADORA1, CRTAC1, IL1A, PCSK9, TLR2, and TREM2. (b) GO semantic similarity among the six signature genes quantified using GOSemSim. (c) mRNA-miRNA network. (d) mRNA-transcription factor (TF) network. (e) CTD-derived mRNA-chemical/drug connectivity network. Abbreviations: PPI, protein-protein interaction; GO, Gene Ontology; TF, transcription factor; CTD, Comparative Toxicogenomics Database.

Immune landscape and therapy-related computational features across PEM risk groups

High-risk tumors had lower StromalScore, ImmuneScore, and ESTIMATEScore and higher Tumor Purity (all $p < 0.001$; Figure 10A). RiskScore correlated negatively with these stromal/immune scores and TIDE and positively with Tumor Purity and TMB; TMB was also higher in the high-risk group (Figure 10b-c). ssGSEA identified 17 immune-cell subsets differing between risk groups ($p < 0.05$; Figure 10d). These subsets were broadly positively correlated within each group (Figure 10e), and their associations with the six signature genes differed by risk stratum (Figure 10f).

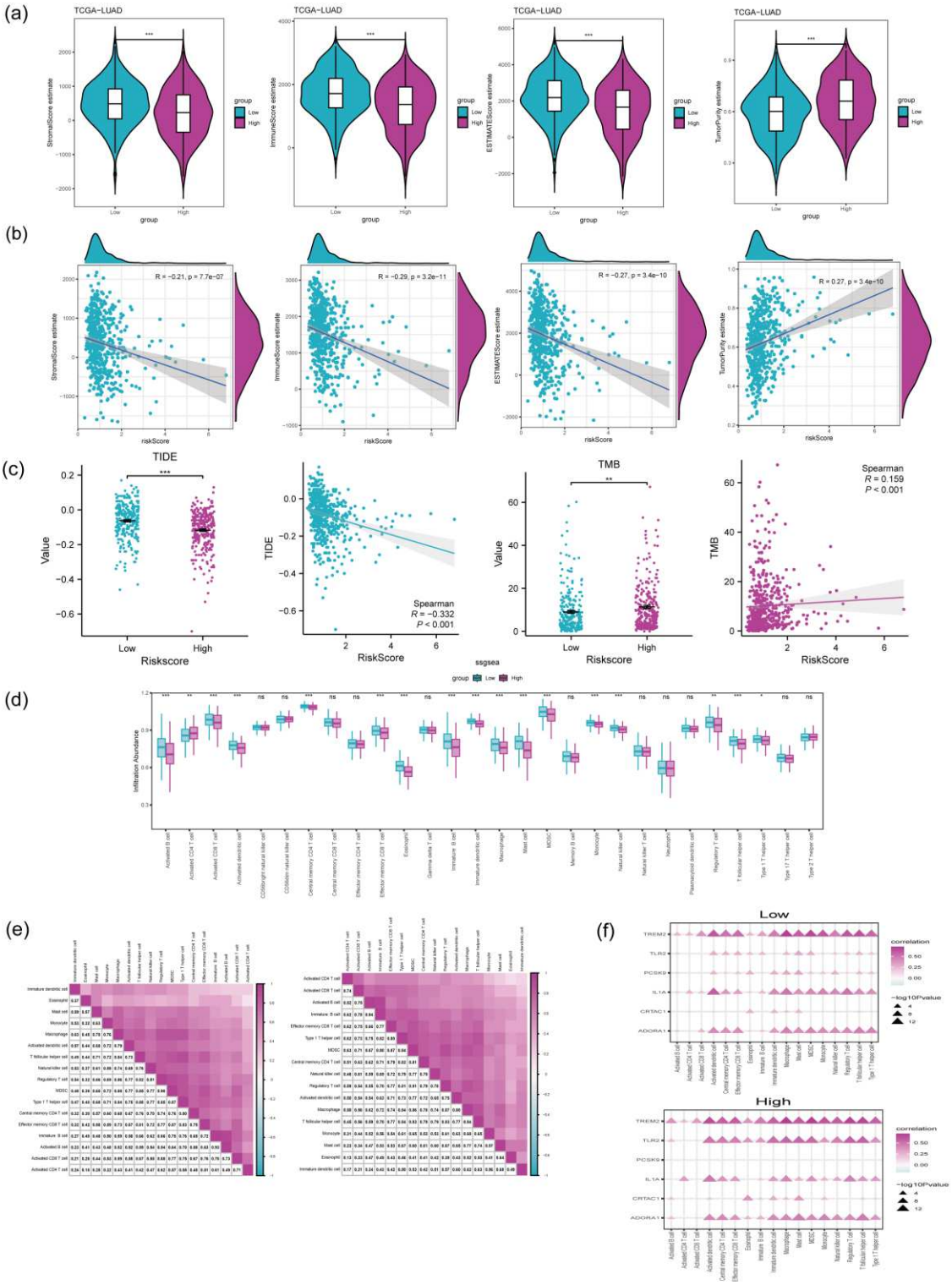


Fig. 10 Immune landscape, therapy relevance, and infiltration patterns between PEM risk groups in TCGA-LUAD. (a) ESTIMATE-derived StromalScore, ImmuneScore, ESTIMATEScore, and TumorPurity compared between low- and high-RiskScore groups. (b) Scatter plots showing Spearman correlations between RiskScore and each ESTIMATE metric. (c) TIDE scores and tumor mutation burden (TMB) in low- and high-RiskScore groups and their correlations with RiskScore. (d) ssGSEA-derived infiltration levels of 28 immune cell subsets in low- and high-RiskScore tumors; significance codes are ns, $p \geq 0.05$; *$p < 0.05$; **$p < 0.01$; ***$p < 0.001$. (e) Correlation heatmaps depicting pairwise relationships among 17 differentially abundant immune cell subsets within low- and high-RiskScore groups. (f) Bubble plots showing correlations between the six signature genes (ADORA1, CRTAC1, IL1A, PCSK9, TLR2, TREM2) and the 17 immune cell subsets in low- and high-RiskScore tumors, with color indicating correlation strength and point size indicating statistical significance.

Prognostic and diagnostic evaluation of the six signature genes

Using the analysis-specific complete-case set for gene-level survival analyses (n = 530), univariable Cox regression showed that higher expression of CRTAC1 (HR = 0.678, 95% CI: 0.506–0.908; P = 0.009), TLR2 (HR = 0.680, 95% CI: 0.508–0.910; P = 0.009), and TREM2 (HR = 0.700, 95% CI: 0.524–0.935; P = 0.015) was associated with a lower risk of death. In contrast, higher PCSK9 expression was associated with a higher risk of death (HR = 1.477, 95% CI: 1.106–1.972; P = 0.008). ADORA1 (HR = 1.123, 95% CI: 0.843–1.495; P = 0.429) and IL1A (HR = 0.991, 95% CI: 0.744–1.320; P = 0.949) were not significantly associated with overall survival (Figure 11a; Supplementary Table S12).

Consistent with the Cox regression results, Kaplan–Meier analysis showed better overall survival in patients with higher CRTAC1, TLR2, and TREM2 expression and poorer survival in those with higher PCSK9 expression, whereas ADORA1 and IL1A showed no significant survival differences (Figure 11b). ROC analysis for distinguishing LUAD tumors from adjacent non-tumor tissues showed the highest AUC for CRTAC1 (AUC = 0.972, 95% CI: 0.960–0.984), followed by PCSK9 (AUC = 0.900, 95% CI: 0.874–0.925), IL1A (AUC = 0.870, 95% CI: 0.837–0.903), TLR2 (AUC = 0.757, 95% CI: 0.716–0.799), TREM2 (AUC = 0.691, 95% CI: 0.627–0.755), and ADORA1 (AUC = 0.493, 95% CI: 0.442–0.543) (Figure 11c; Supplementary Table S12).

RT–qPCR validation of the six signature genes in paired LUAD tumor and adjacent tissues

RT–qPCR analysis of 19 paired LUAD tumor and adjacent non-tumor tissues showed significantly lower tumor expression of CRTAC1 ($p < 0.0001$), IL1A ($p < 0.0001$), and PCSK9 ($p < 0.001$), whereas ADORA1 ($p = 0.312$), TLR2 ($p = 0.515$), and TREM2 ($p = 0.953$) showed no significant tumor–adjacent differences. After Benjamini–Hochberg correction, CRTAC1, IL1A, and PCSK9 remained significantly downregulated in tumor tissues (FDR q < 0.05; Figure 12a–b; Supplementary Table S15).

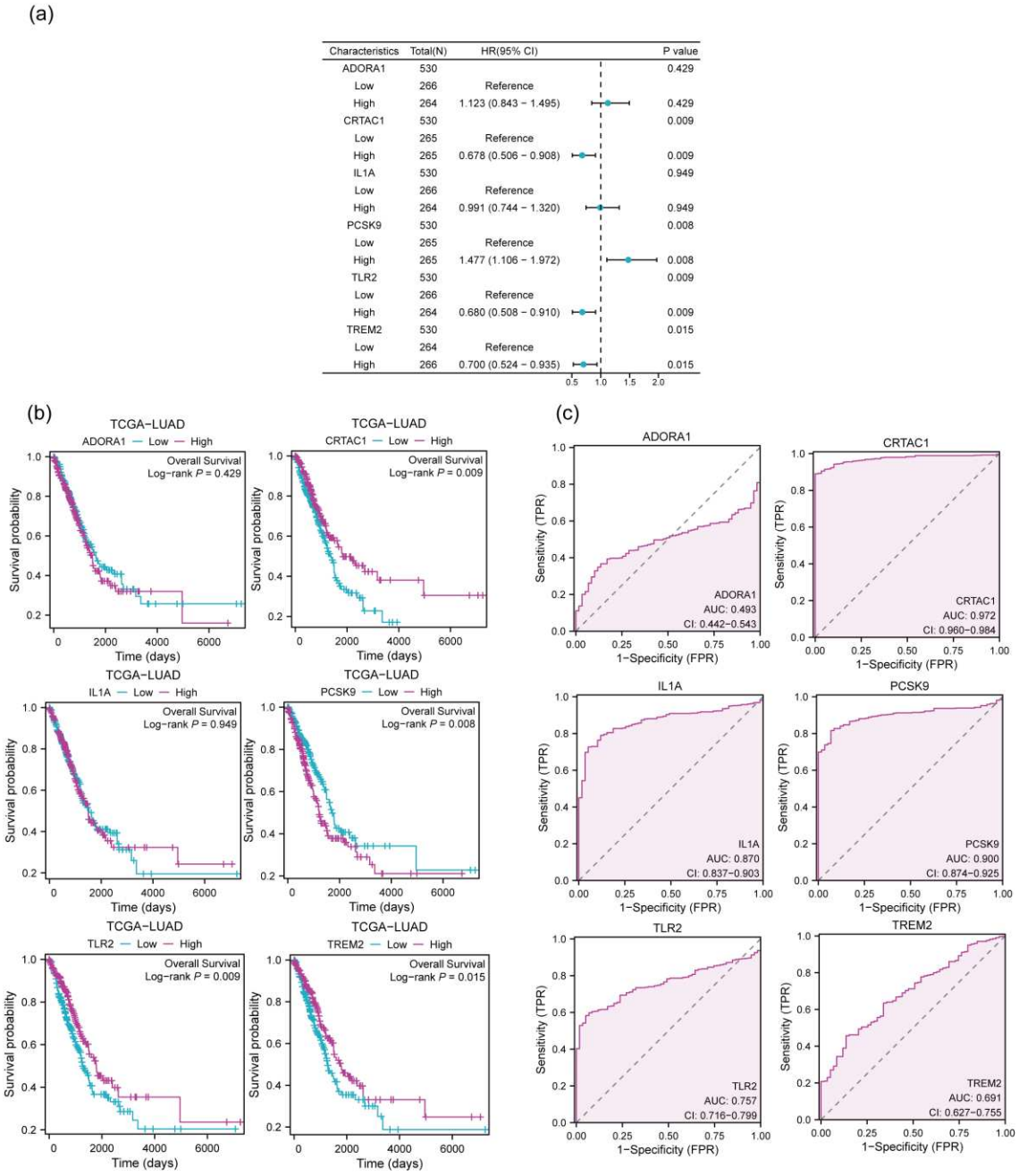


Fig. 11 Prognostic and diagnostic evaluation of the six PEM signature genes in TCGA-LUAD. Gene-level survival analyses in panels (a) and (b) used the analysis-specific complete-case set (n = 530), defined separately from the multivariable model analysis set. (a) Forest plot showing gene-level univariable Cox regression results for ADORA1, CRTAC1, IL1A, PCSK9, TLR2, and TREM2. Patients were divided into high- and low-expression groups according to the median expression of each gene, with the low-expression group as the reference. Hazard ratios (HRs), 95% confidence intervals (CIs), and P values are shown. (b) Kaplan–Meier curves comparing overall survival between the high- and low-expression groups for each signature gene; P values were calculated using log-rank tests. (c) Receiver operating characteristic (ROC) curves

showing the performance of the six signature genes in distinguishing LUAD tumors from adjacent non-tumor tissues, with corresponding areas under the curve (AUCs) and 95% CIs.

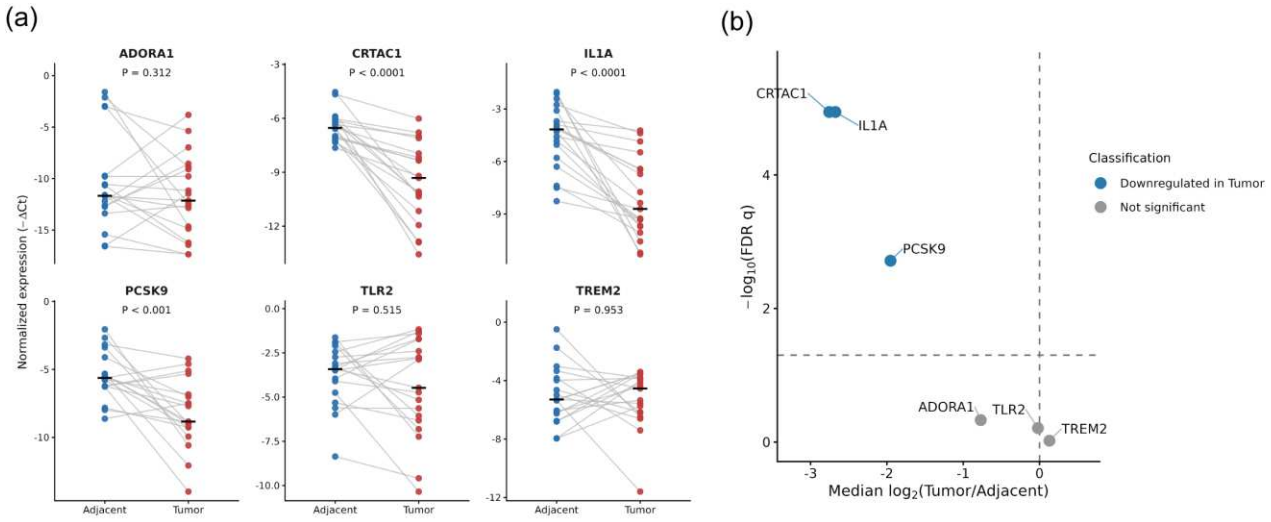


Fig. 12 RT-qPCR validation of the six signature genes in 19 paired LUAD tumor and adjacent non-tumor tissues.(a) Paired normalized log2 expression (−ΔCt) of the six signature genes in matched adjacent and tumor tissues. Each point represents one patient, with matched pairs connected by gray lines; black bars indicate the median. P values were calculated using two-sided paired Wilcoxon signed-rank tests: ADORA1, $p = 0.312$; CRTAC1, $p < 0.0001$; IL1A, $p < 0.0001$; PCSK9, $p < 0.001$; TLR2, $p = 0.515$; and TREM2, $p = 0.953$. (b) Summary of median log2(Tumor/Adjacent) expression changes and −log10(FDR q) values. FDR q values were obtained using Benjamini–Hochberg correction across the six genes. Dashed lines indicate FDR q = 0.05 and log2(Tumor/Adjacent) = 0. Blue denotes significant tumor downregulation, and gray denotes nonsignificant differences.

Discussion

Lung adenocarcinoma (LUAD) remains the predominant histological subtype of non-small-cell lung cancer[43] and exhibits substantial inter-tumoral heterogeneity, including variation in metabolic and immune states[44]. Accumulating evidence indicates that pyroptosis and metabolic reprogramming are closely intertwined with tumor behavior and immune escape[45-47]. In this study, we integrated multi-cohort transcriptomic data with genomic, regulatory, and immune-context analyses to define a pyroptosis–energy metabolism (PEM) framework in LUAD. We identified 28 PEM module genes, resolved three molecular subtypes with different survival outcomes, developed a six-gene prognostic signature comprising ADORA1, CRTAC1, IL1A, PCSK9, TLR2, and TREM2.We further examined the prognostic and diagnostic performance of each signature gene and assessed their expression in 19 paired LUAD and adjacent non-tumor tissues by RT-qPCR. CRTAC1, IL1A, and PCSK9 were significantly downregulated in the paired tissues, whereas ADORA1, TLR2, and TREM2 showed no significant tumor-adjacent differences.

Considering inflammatory cell death and metabolic remodeling together may provide a more integrated view of PEM-related heterogeneity in LUAD[7,10,11]. The three PEM-defined subtypes showed distinct expression patterns and survival outcomes, suggesting heterogeneity in

inflammatory and metabolic programs, although the biological basis of these subtype differences requires further validation. Functional analyses of the prognostic genes implicated hypoxia responses, lipid-related processes, extracellular-matrix remodeling, secretion, and innate immune activation. These observations suggest that pyroptosis-associated inflammatory signaling and metabolic adaptation may jointly shape LUAD phenotypes[48,49], however, the present transcriptomic analyses are associative and do not establish a causal PEM pathway.

Gene-level analyses revealed heterogeneous prognostic associations among the six signature genes. Higher expression of CRTAC1, TLR2, and TREM2 was associated with a lower risk of death, whereas higher PCSK9 expression was associated with a higher risk; ADORA1 and IL1A were not significantly associated with overall survival when evaluated individually. The absence of significant individual prognostic associations for ADORA1 and IL1A does not preclude their contribution to the multigene signature, because coefficients in a multivariable Cox model reflect effects conditional on the other model components. Accordingly, the prognostic value of the signature reflects the combined information provided by the six genes rather than the univariable effect of any single gene.

Among the six signature genes, CRTAC1 showed the most consistent findings across the different analytical levels. Higher CRTAC1 expression was associated with a lower risk of death in the gene-level Cox analysis and better overall survival in Kaplan-Meier analysis, while its diagnostic AUC reached 0.972. Transcriptomic analyses showed lower CRTAC1 expression in LUAD tumor tissues than in normal tissues, and RT–qPCR analysis likewise showed lower expression in tumor tissues than in paired adjacent non-tumor tissues. Previous studies in LUAD have reported reduced CRTAC1 expression in tumor tissues, with lower expression associated with poorer prognosis. Functional studies further suggest that CRTAC1 suppresses LUAD cell proliferation, migration, and invasion, partly through inhibition of integrin/FAK signaling.[50,51]. Taken together, these findings support CRTAC1 as the most consistent biomarker candidate identified in this study, although further clinical and functional evaluation is required.

PCSK9 showed a context-dependent expression pattern across datasets. Its expression was lower in LUAD tumors than in normal tissues in TCGA-LUAD and GSE32863, whereas higher tumor expression was observed in GSE31210. Paired RT-qPCR analysis also showed lower PCSK9 expression in tumor tissues. In survival analyses, however, higher PCSK9 expression within LUAD tumors was associated with poorer overall survival, consistent with its positive coefficient in the six-gene risk model. These findings are not necessarily contradictory, because tumor-versus-normal differential expression and within-tumor prognostic association address different biological questions. Given the reported roles of PCSK9 in cholesterol metabolism, antigen presentation, and antitumor immunity[52-54], PCSK9 may link lipid metabolic regulation with tumor immunity. Nevertheless, the variability in its expression across cohorts warrants further validation in LUAD.

The remaining signature genes appear more context dependent and may reflect microenvironmental or cell-composition effects rather than uniform tumor-cell expression. Adenosinergic signaling is an established immunoregulatory component of the tumor microenvironment[55], and ADORA1 has been implicated in hypoxia-associated purinergic signaling and immune suppression[56,57]. Although ADORA1 was not significantly associated with overall survival in the gene-level analysis, its positive coefficient in the six-gene model may reflect information captured in combination with the other signature genes or risk-associated microenvironmental states. IL1A likewise contributed positively to the prognostic model but was

downregulated in paired tumors. The absence of a significant gene-level survival association suggests that the contribution of IL1A to the combined signature may depend on interactions with other molecular features or differences in cellular context. As an inflammatory marker, IL1A can participate in inflammatory signaling and myeloid recruitment.[58,59]. TLR2 and TREM2 were favorable prognostic correlates in the bulk-transcriptomic analyses but have dual or cell-state-specific roles in tumor immunity: TLR2 can support innate immune activation yet also sustain tumor-promoting inflammation[60,61], whereas TREM2-expressing tumor-associated macrophages have been linked to immunosuppressive myeloid states and modulation of anti-PD-1 responses[62,63]. The absence of significant tumor–adjacent differences for ADORA1, TLR2, and TREM2 further supports cell-type-resolved investigation.

The immune and regulatory analyses further contextualized the prognostic signature. High-risk tumors showed lower stromal and immune scores, higher tumor purity and TMB, and lower TIDE scores, indicating that genomic immunogenicity, computational immune-escape estimates, and immune-cell abundance did not vary in a uniformly concordant manner. Because TMB and TIDE are surrogate computational measures rather than direct indicators of treatment response, these findings should not be interpreted as evidence of superior immunotherapy efficacy without validation in treated cohorts. The PPI, functional-similarity, mRNA–miRNA, and mRNA–TF analyses provided complementary hypotheses regarding regulatory coordination, while CTD-derived chemical–gene associations served only as a hypothesis-generating drug-connectivity map rather than evidence of therapeutic efficacy[38]. These analyses provide further evidence for the biological relevance of the six-gene signature and help define the potential roles of its individual components. CRTAC1 and PCSK9 may be prioritized for further biomarker and mechanistic investigation, whereas ADORA1, IL1A, TLR2, and TREM2 require more detailed evaluation in specific cellular and microenvironmental settings.

Several limitations should be acknowledged. The RT–qPCR cohort was modest, comprising 19 paired specimens, and ADORA1, TLR2, and TREM2 did not show significant tumor-versus-adjacent differences. In addition, bulk tissue transcriptomic data reflect gene expression from mixed cell populations and therefore cannot determine whether the observed signals arise primarily from tumor, stromal, or immune cells. This issue is particularly relevant to the interpretation of IL1A, TLR2, and TREM2, whose expression may be influenced by the cellular composition of the tumor microenvironment. Moreover, the PPI, miRNA, TF, and drug-connectivity analyses are partly based on curated or predicted associations and therefore require functional validation. Larger multicenter tissue cohorts, spatial or single-cell analyses, and functional studies will be needed to clarify the cellular sources and biological roles of the identified genes and to investigate the biological basis of the observed PEM-related associations.

In conclusion, this study identified a six-gene PEM-related signature associated with overall survival and the tumor immune environment in LUAD. CRTAC1 showed the most consistent evidence across transcriptomic datasets, survival analyses, diagnostic evaluation, and paired clinical tissues, with lower expression in tumors and higher expression associated with better survival. These findings support further investigation of CRTAC1 and the other signature genes as biomarkers related to pyroptosis, energy metabolism, and immune regulation in LUAD.

References

[1] F. Bray, M. Laversanne, H. Sung, J. Ferlay, R.L. Siegel, I. Soerjomataram, et al., Global cancer statistics 2022: globocan estimates of incidence and mortality worldwide for 36 cancers in 185 countries, CA: a cancer journal for clinicians 74 (3) (2024) 229-263, https://doi.org/10.3322/caac.21834.

[2] A.G. Nicholson, M.S. Tsao, M.B. Beasley, A.C. Borczuk, E. Brambilla, W.A. Cooper, et al., The 2021 who classification of lung tumors: impact of advances since 2015, Journal of thoracic oncology : official publication of the International Association for the Study of Lung Cancer 17 (3) (2022) 362-387, https://doi.org/10.1016/j.jtho.2021.11.003.

[3] B.C. Cho, S. Lu, E. Felip, A.I. Spira, N. Girard, J. Lee, et al., Amivantamab plus lazertinib in previously untreated egfr-mutated advanced nsclc, The New England journal of medicine 391 (16) (2024) 1486-1498, https://doi.org/10.1056/NEJMoa2403614.

[4] M.V. Verschueren, B.J. Peters, L.T. Bloem, V.R. Kruik, E.B. Uitvlugt, A.R. Bijsmans, et al., Pembrolizumab plus chemotherapy per pd-l1 stratum in patients with metastatic non-small cell lung cancer: real-world effectiveness versus trial efficacy, Clin. Lung Cancer 25 (2) (2024) 119-127, https://doi.org/10.1016/j.cllc.2023.12.011.

[5] K. Wang, Q. Sun, X. Zhong, M. Zeng, H. Zeng, X. Shi, et al., Structural mechanism for gsdmd targeting by autoprocessed caspases in pyroptosis, Cell 180 (5) (2020) 941-955, https://doi.org/10.1016/j.cell.2020.02.002.

[6] K.V. Swanson, M. Deng, J.P. Ting, The nlrp3 inflammasome: molecular activation and regulation to therapeutics, Nature reviews. Immunology 19 (8) (2019) 477-489, https://doi.org/10.1038/s41577-019-0165-0.

[7] C.L. Evavold, J. Ruan, Y. Tan, S. Xia, H. Wu, J.C. Kagan, The pore-forming protein gasdermin d regulates interleukin-1 secretion from living macrophages, Immunity 48 (1) (2018) 35-44, https://doi.org/10.1016/j.immuni.2017.11.013.

[8] C. Chang, J. Qiu, D. O'Sullivan, M.D. Buck, T. Noguchi, J.D. Curtis, et al., Metabolic competition in the tumor microenvironment is a driver of cancer progression, Cell 162 (6) (2015) 1229-1241, https://doi.org/10.1016/j.cell.2015.08.016.

[9] B. Allard, D. Allard, L. Buisseret, J. Stagg, The adenosine pathway in immuno-oncology, Nature reviews. Clinical oncology 17 (10) (2020) 611-629, https://doi.org/10.1038/s41571-020-0382-2.

[10] G.M. Tannahill, A.M. Curtis, J. Adamik, E.M. Palsson-Mcdermott, A.F. Mcgettrick, G. Goel, et al., Succinate is an inflammatory signal that induces il-1β through hif-1α, Nature 496 (7444) (2013) 238-242, https://doi.org/10.1038/nature11986.

[11] Z. Wang, Z. Gu, W. Mo, H. Zhang, Lactate metabolic checkpoint in immuno-oncology: mechanisms and therapeutic implications, Cancer Lett. 633 (2025) 218038, https://doi.org/10.1016/j.canlet.2025.218038.

[12] R. Edgar, M. Domrachev, A.E. Lash, Gene expression omnibus: ncbi gene expression and hybridization array data repository, Nucleic. Acids. Res. 30 (1) (2002) 207-210, https://doi.org/10.1093/nar/30.1.207.

[13] P. Langfelder, S. Horvath, Wgcna: an r package for weighted correlation network analysis, BMC Bioinformatics 9 (2008) 559, https://doi.org/10.1186/1471-2105-9-559.

[14] S. Hänzelmann, R. Castelo, J. Guinney, Gsva: gene set variation analysis for microarray and rna-seq data, BMC Bioinformatics 14 (2013) 7, https://doi.org/10.1186/1471-2105-14-7.

[15] R. Tibshirani, The lasso method for variable selection in the cox model, Stat. Med. 16 (4) (1997) 385-395, https://doi.org/10.1002/(sici)1097-0258(19970228)16:4<385::aid-sim380>3.0.co;2-3.
[16] A. Subramanian, R. Narayan, S.M. Corsello, D.D. Peck, T.E. Natoli, X. Lu, et al., A next generation connectivity map: l1000 platform and the first 1,000,000 profiles, Cell 171 (6) (2017) 1437-1452, https://doi.org/10.1016/j.cell.2017.10.049.
[17] A. Colaprico, T.C. Silva, C. Olsen, L. Garofano, C. Cava, D. Garolini, et al., Tcgabiolinks: an r/bioconductor package for integrative analysis of tcga data, Nucleic. Acids. Res. 44 (8) (2016) e71, https://doi.org/10.1093/nar/gkv1507.
[18] J. Gao, B.A. Aksoy, U. Dogrusoz, G. Dresdner, B. Gross, S.O. Sumer, et al., Integrative analysis of complex cancer genomics and clinical profiles using the cbioportal, Sci. Signal. 6 (269) (2013) pl1, https://doi.org/10.1126/scisignal.2004088.
[19] D.C. Koboldt, Q. Zhang, D.E. Larson, D. Shen, M.D. Mclellan, L. Lin, et al., Varscan 2: somatic mutation and copy number alteration discovery in cancer by exome sequencing, Genome Res. 22 (3) (2012) 568-576, https://doi.org/10.1101/gr.129684.111.
[20] C.H. Mermel, S.E. Schumacher, B. Hill, M.L. Meyerson, R. Beroukhim, G. Getz, Gistic2.0 facilitates sensitive and confident localization of the targets of focal somatic copy-number alteration in human cancers, Genome Biol. 12 (4) (2011) R41, https://doi.org/10.1186/gb-2011-12-4-r41.
[21] H. Okayama, T. Kohno, Y. Ishii, Y. Shimada, K. Shiraishi, R. Iwakawa, et al., Identification of genes upregulated in alk-positive and egfr/kras/alk-negative lung adenocarcinomas, Cancer Res. 72 (1) (2012) 100-111, https://doi.org/10.1158/0008-5472.CAN-11-1403.
[22] S.A. Selamat, B.S. Chung, L. Girard, W. Zhang, Y. Zhang, M. Campan, et al., Genome-scale analysis of dna methylation in lung adenocarcinoma and integration with mrna expression, Genome Res. 22 (7) (2012) 1197-1211, https://doi.org/10.1101/gr.132662.111.
[23] G. Stelzer, N. Rosen, I. Plaschkes, S. Zimmerman, M. Twik, S. Fishilevich, et al., The genecards suite: from gene data mining to disease genome sequence analyses, Current protocols in bioinformatics 54 (2016) 1-30, https://doi.org/10.1002/cpbi.5.
[24] B. Zhang, S. Horvath, A general framework for weighted gene co-expression network analysis, Stat. Appl. Genet. Mol. Biol. 4 (2005) Article17, https://doi.org/10.2202/1544-6115.1128.
[25] M.D. Wilkerson, D.N. Hayes, Consensusclusterplus: a class discovery tool with confidence assessments and item tracking, Bioinformatics (Oxford, England) 26 (12) (2010) 1572-1573, https://doi.org/10.1093/bioinformatics/btq170.
[26] M.E. Ritchie, B. Phipson, D. Wu, Y. Hu, C.W. Law, W. Shi, et al., Limma powers differential expression analyses for rna-sequencing and microarray studies, Nucleic. Acids. Res. 43 (7) (2015) e47, https://doi.org/10.1093/nar/gkv007.
[27] G. Yu, L. Wang, Y. Han, Q. He, Clusterprofiler: an r package for comparing biological themes among gene clusters, Omics : a journal of integrative biology 16 (5) (2012) 284-287, https://doi.org/10.1089/omi.2011.0118.
[28] M. Kanehisa, S. Goto, Kegg: kyoto encyclopedia of genes and genomes, Nucleic. Acids. Res. 28 (1) (2000) 27-30, https://doi.org/10.1093/nar/28.1.27.
[29] A. Subramanian, P. Tamayo, V.K. Mootha, S. Mukherjee, B.L. Ebert, M.A. Gillette, et al., Gene set enrichment analysis: a knowledge-based approach for interpreting genome-wide expression profiles, Proc. Natl. Acad. Sci. U. S. A. 102 (43) (2005) 15545-15550, https://doi.org/10.1073/pnas.0506580102.

[30] A. Liberzon, A. Subramanian, R. Pinchback, H. Thorvaldsdóttir, P. Tamayo, J.P. Mesirov, Molecular signatures database (msigdb) 3.0, Bioinformatics (Oxford, England) 27 (12) (2011) 1739-1740, https://doi.org/10.1093/bioinformatics/btr260.
[31] D. Szklarczyk, A.L. Gable, D. Lyon, A. Junge, S. Wyder, J. Huerta-Cepas, et al., String v11: protein-protein association networks with increased coverage, supporting functional discovery in genome-wide experimental datasets, Nucleic. Acids. Res. 47 (D1) (2019) D607-D613, https://doi.org/10.1093/nar/gky1131.
[32] P. Shannon, A. Markiel, O. Ozier, N.S. Baliga, J.T. Wang, D. Ramage, et al., Cytoscape: a software environment for integrated models of biomolecular interaction networks, Genome Res. 13 (11) (2003) 2498-2504, https://doi.org/10.1101/gr.1239303.
[33] G. Yu, Gene ontology semantic similarity analysis using gosemsim, Methods in molecular biology (Clifton, N.J.) 2117 (2020) 207-215, https://doi.org/10.1007/978-1-0716-0301-7_11.
[34] Y. Chen, X. Wang, Mirdb: an online database for prediction of functional microrna targets, Nucleic. Acids. Res. 48 (D1) (2020) D127-D131, https://doi.org/10.1093/nar/gkz757.
[35] J. Li, S. Liu, H. Zhou, L. Qu, J. Yang, Starbase v2.0: decoding mirna-cerna, mirna-ncrna and protein-rna interaction networks from large-scale clip-seq data, Nucleic. Acids. Res. 42 (Database issue) (2014) D92-D97, https://doi.org/10.1093/nar/gkt1248.
[36] J. Huang, W. Zheng, P. Zhang, Q. Lin, Z. Chen, J. Xuan, et al., Chipbase v3.0: the encyclopedia of transcriptional regulations of non-coding rnas and protein-coding genes, Nucleic. Acids. Res. 51 (D1) (2023) D46-D56, https://doi.org/10.1093/nar/gkac1067.
[37] Q. Zhang, W. Liu, H. Zhang, G. Xie, Y. Miao, M. Xia, et al., Htftarget: a comprehensive database for regulations of human transcription factors and their targets, Genomics, proteomics & bioinformatics 18 (2) (2020) 120-128, https://doi.org/10.1016/j.gpb.2019.09.006.
[38] A.P. Davis, C.J. Grondin, R.J. Johnson, D. Sciaky, J. Wiegers, T.C. Wiegers, et al., Comparative toxicogenomics database (ctd): update 2021, Nucleic. Acids. Res. 49 (D1) (2021) D1138-D1143, https://doi.org/10.1093/nar/gkaa891.
[39] K. Yoshihara, M. Shahmoradgoli, E. Martínez, R. Vegesna, H. Kim, W. Torres-Garcia, et al., Inferring tumour purity and stromal and immune cell admixture from expression data, Nat. Commun. 4 (2013) 2612, https://doi.org/10.1038/ncomms3612.
[40] P. Jiang, S. Gu, D. Pan, J. Fu, A. Sahu, X. Hu, et al., Signatures of t cell dysfunction and exclusion predict cancer immunotherapy response, Nat. Med. 24 (10) (2018) 1550-1558, https://doi.org/10.1038/s41591-018-0136-1.
[41] P. Charoentong, F. Finotello, M. Angelova, C. Mayer, M. Efremova, D. Rieder, et al., Pan-cancer immunogenomic analyses reveal genotype-immunophenotype relationships and predictors of response to checkpoint blockade, Cell Rep. 18 (1) (2017) 248-262, https://doi.org/10.1016/j.celrep.2016.12.019.
[42] D.A. Barbie, P. Tamayo, J.S. Boehm, S.Y. Kim, S.E. Moody, I.F. Dunn, et al., Systematic rna interference reveals that oncogenic kras-driven cancers require tbk1, Nature 462 (7269) (2009) 108-112, https://doi.org/10.1038/nature08460.
[43] M. Zheng, Classification and pathology of lung cancer, Surg. Oncol. Clin. N. Am. 25 (3) (2016) 447-468, https://doi.org/10.1016/j.soc.2016.02.003.
[44] D. Hanahan, Hallmarks of cancer: new dimensions, Cancer Discov. 12 (1) (2022) 31-46, https://doi.org/10.1158/2159-8290.CD-21-1059.

[45] D.S. Chen, I. Mellman, Oncology meets immunology: the cancer-immunity cycle, Immunity 39 (1) (2013) 1-10, https://doi.org/10.1016/j.immuni.2013.07.012.
[46] Y. Fang, S. Tian, Y. Pan, W. Li, Q. Wang, Y. Tang, et al., Pyroptosis: a new frontier in cancer, Biomedicine & pharmacotherapy = Biomedecine & pharmacotherapie 121 (2020) 109595, https://doi.org/10.1016/j.biopha.2019.109595.
[47] I. Mellman, D.S. Chen, T. Powles, S.J. Turley, The cancer-immunity cycle: indication, genotype, and immunotype, Immunity 56 (10) (2023) 2188-2205, https://doi.org/10.1016/j.immuni.2023.09.011.
[48] T. Chen, Y. Li, X. Long, A new frontier in cancer therapy: inositol-requiring enzyme 1 alpha (ire1α) and taxane-induced pyroptosis, Molecular biomedicine 6 (1) (2025) 86, https://doi.org/10.1186/s43556-025-00336-w.
[49] M.V. Pinzon-Fernandez, J.S. Saavedra-Torres, N.A. Lopez Garzon, J.S. Pachon-Bueno, F.J. Tamayo-Giraldo, M.C. Rojas Gomez, et al., Nlrp3 and beyond: inflammasomes as central cellular hub and emerging therapeutic target in inflammation and disease, Front. Immunol. 16 (2025) 1624770, https://doi.org/10.3389/fimmu.2025.1624770.
[50] L. Tan, H. Zhang, Y. Ding, Y. Huang, D. Sun, Crtac1 identified as a promising diagnosis and prognostic biomarker in lung adenocarcinoma, Sci. Rep. 14 (1) (2024) 11223, https://doi.org/10.1038/s41598-024-61804-x.
[51] Y. Liu, Y. Chang, H. Li, J. Wang, H. Jin, C. Huang, et al., Crtac1 inhibits progression of lung adenocarcinoma by suppressing integrin/fak signaling, Oncogene 45 (10) (2026) 946-960, https://doi.org/10.1038/s41388-026-03691-2.
[52] Q. Wang, Z. Chen, X. Lu, H. Lin, H. Feng, N. Weng, et al., Methionine metabolism dictates pcsk9 expression and antitumor potency of pd-1 blockade in mss colorectal cancer, Advanced science (Weinheim, Baden-Wurttemberg, Germany) 12 (19) (2025) e2501623, https://doi.org/10.1002/advs.202501623.
[53] H. Wang, X. Zhang, Y. Zhang, T. Shi, Y. Zhang, X. Song, et al., Targeting pcsk9 to upregulate mhc-ii on the surface of tumor cells in tumor immunotherapy, BMC Cancer 24 (1) (2024) 445, https://doi.org/10.1186/s12885-024-12148-2.
[54] Y. Wang, X. Fang, J. Liu, X. Lv, K. Lu, Y. Lu, et al., Pcsk9 in t-cell function and the immune response, Biomark. Res. 12 (1) (2024) 163, https://doi.org/10.1186/s40364-024-00712-8.
[55] C. Zhang, K. Wang, H. Wang, Adenosine in cancer immunotherapy: taking off on a new plane, Biochim. Biophys. Acta-Rev. Cancer 1878 (6) (2023) 189005, https://doi.org/10.1016/j.bbcan.2023.189005.
[56] L. Pang, K.T. Ng, J. Liu, W.O. Yeung, J. Zhu, T.S. Chiu, et al., Plasmacytoid dendritic cells recruited by hif-1α/eado/adora1 signaling induce immunosuppression in hepatocellular carcinoma, Cancer Lett. 522 (2021) 80-92, https://doi.org/10.1016/j.canlet.2021.09.022.
[57] R.C. Augustin, R.D. Leone, A. Naing, L. Fong, R. Bao, J.J. Luke, Next steps for clinical translation of adenosine pathway inhibition in cancer immunotherapy, J. Immunother. Cancer 10 (2) (2022) e4089, https://doi.org/10.1136/jitc-2021-004089.
[58] A. Mantovani, I. Barajon, C. Garlanda, Il-1 and il-1 regulatory pathways in cancer progression and therapy, Immunol. Rev. 281 (1) (2018) 57-61, https://doi.org/10.1111/imr.12614.
[59] A. Mantovani, C.A. Dinarello, M. Molgora, C. Garlanda, Interleukin-1 and related cytokines in the regulation of inflammation and immunity, Immunity 50 (4) (2019) 778-795, https://doi.org/10.1016/j.immuni.2019.03.012.

[60] T. Kawai, S. Akira, Toll-like receptors and their crosstalk with other innate receptors in infection and immunity, Immunity 34 (5) (2011) 637-650, https://doi.org/10.1016/j.immuni.2011.05.006.
[61] A. Di Lorenzo, E. Bolli, L. Tarone, F. Cavallo, L. Conti, Toll-like receptor 2 at the crossroad between cancer cells, the immune system, and the microbiota, International journal of molecular sciences 21 (24) (2020) 9418, https://doi.org/10.3390/ijms21249418.
[62] M. Molgora, E. Esaulova, W. Vermi, J. Hou, Y. Chen, J. Luo, et al., Trem2 modulation remodels the tumor myeloid landscape enhancing anti-pd-1 immunotherapy, Cell 182 (4) (2020) 886-900, https://doi.org/10.1016/j.cell.2020.07.013.
[63] Z.Z. Ji, M.K. Chan, A.S. Chan, K. Leung, X. Jiang, K. To, et al., Tumour-associated macrophages: versatile players in the tumour microenvironment, Front. Cell. Dev. Biol. 11 (2023) 1261749, https://doi.org/10.3389/fcell.2023.1261749.

Author Contributions

Kang Luo: Conceptualization, Methodology, Formal analysis, Visualization, Writing – original draft. Guangyuan Guo: Methodology, Software, Formal analysis, Data curation, Validation, Visualization. Haoyu Liu: Formal analysis, Validation, Data curation, Investigation. Wenwen Huang: Investigation, Validation, Data curation. Xiang Gao: Investigation, Validation, Data curation. Yunfei Shi: Investigation, Resources, Data curation. Yiming Han: Investigation, Resources, Validation. Shen Han: Resources, Supervision, Writing – review & editing. Mingyao Meng: Conceptualization, Supervision, Project administration, Writing – review & editing. Bingrong Zheng: Conceptualization, Supervision, Project administration, Funding acquisition, Writing – review & editing. All authors read and approved the final manuscript. Kang Luo, Guangyuan Guo, and Haoyu Liu contributed equally to this work.

Funding

This work was supported by the National Natural Science Foundation of China (No. 82260063), the Clinical Medical Research Center for Cardiovascular Disease of Yunnan Province (No. 202405AJ310005), the Yunnan Fundamental Research Projects (Grant No. 202401AT070260), and the Kunming Medical University Leading Clinical Research Project (Grant No. 2025MR067).

Data Availability

The publicly available datasets and external resources used in this study are accessible from the following repositories. TCGA-LUAD RNA-sequencing, somatic mutation, copy-number, and primary clinical data were obtained from the National Cancer Institute Genomic Data Commons (GDC), project Lung Adenocarcinoma (TCGA-LUAD), under project ID TCGA-LUAD (https://portal.gdc.cancer.gov/projects/TCGA-LUAD). Matched clinical information used for complementary analyses was retrieved from the TCGA Lung Adenocarcinoma (LUAD) cohort in UCSC Xena (https://xenabrowser.net/datapages/?cohort=TCGA+Lung+Adenocarcinoma+%28LUAD%29). Tumor mutational burden (TMB) data were obtained from the cBioPortal Lung Adenocarcinoma (TCGA, PanCancer Atlas) study (study ID: luad_tcga_pan_can_atlas_2018) (https://www.cbioportal.org/study/summary?id=luad_tcga_pan_can_atlas_2018).

Independent transcriptomic datasets were obtained from the NCBI Gene Expression Omnibus (GEO): “Gene expression data for pathological stage I-II lung adenocarcinomas”, accession GSE31210, platform GPL570 (https://www.ncbi.nlm.nih.gov/geo/query/acc.cgi?acc=GSE31210), and “Gene expression analysis of lung adenocarcinoma and matched adjacent non-tumor lung tissue”, accession GSE32863, platform GPL6884 (https://www.ncbi.nlm.nih.gov/geo/query/acc.cgi?acc=GSE32863).

GeneCards was queried using the terms “pyroptosis” (https://www.genecards.org/search/results?q=pyroptosis) and “energy metabolism” (https://www.genecards.org/search/results?q=energy%20metabolism) to retrieve protein-coding genes with a relevance score > 0.5; the final 90 PEM-related genes used for downstream analyses are provided in Supplementary Table S2.

Gene sets for enrichment analyses were obtained from the Molecular Signatures Database (MSigDB, release 2022.1.Hs) (https://data.broadinstitute.org/gsea-msigdb/msigdb/release/2022.1.Hs/). GSEA used c2.all.v2022.1.Hs.symbols.gmt (https://data.broadinstitute.org/gsea-msigdb/msigdb/release/2022.1.Hs/c2.all.v2022.1.Hs.symbols.gmt), whereas GSVA used the C2 curated gene set collection retrieved through the msigdbr R package. Protein-protein interaction data for ADORA1, CRTAC1, IL1A, PCSK9, TLR2, and TREM2 were obtained from STRING v11 for Homo sapiens (NCBI taxonomy ID: 9606) using the highest-confidence interaction threshold (score ≥ 0.900) (https://version-11-0.string-db.org/), and the resulting network was visualized using Cytoscape v3.9.1.

Additional online resources used in secondary analyses included the Tumor Immune Dysfunction and Exclusion (TIDE) framework (http://tide.dfci.harvard.edu/) for immune-evasion-related computational scores; miRDB (https://www.mirdb.org/) and ENCORI/starBase (https://rnasysu.com/encori/) for miRNA-target relationships; ChIPBase v3.0 (https://rnasysu.com/chipbase3/) and hTFtarget (https://guolab.wchscu.cn/hTFtarget/) for transcription factor-target relationships; and the Comparative Toxicogenomics Database (CTD) Batch Query resource (https://ctdbase.org/tools/batchQuery.go) for chemical-gene associations.

The RT-qPCR data generated in this study, including experimental conditions, primer sequences, and supporting raw data, are provided in Supplementary Tables S13–S17. Additional de-identified clinical data are not publicly posted because access is subject to applicable institutional and ethical requirements. These data are available from the corresponding author upon reasonable request.

Declarations

Ethical Approval and Accordance

The study protocol was approved by the Ethics Committee of the First Affiliated Hospital of Kunming Medical University (Approval No. (2026) Ethics Review L No. 14) and was conducted in accordance with the Declaration of Helsinki and applicable institutional guidelines and regulations.

Consent to Participate

Written informed consent was obtained from all participants before sample collection.

Consent to Publish

Not applicable.

Competing Interests

The authors declare no competing interests.

Supplementary Files

This is a list of supplementary files associated with this preprint. Click to download.

- SupplementaryTableS2.PyroptosisandEnergyMetabolismRelatedGenesList.docx
- SupplementaryTableS1.LungAdenocarcinomaDatasetInformation.docx
- SupplementaryTableS3.UnivariateCoxRegressionAnalysisofPEMRGsAssociatedwithOSinTCGALUAD.docx
- SupplementaryTableS6.GSEAResultsBetweenHighandLowRiskScoreGroupsinTCGALUAD.docx
- SupplementaryTableS7.GSVAResultsBetweenHighandLowRiskScoreGroupsinTCGALUAD.docx
- SupplementaryTableS9.mRNATFinteractionnetworknodes.docx
- SupplementaryTableS10.mRNAdrugsinteractionnetworknodes.docx
- SupplementaryTableS5.GOandKEGGenrichmentanalysisresultsofPrognosisPEMRGs.docx
- SupplementaryTableS8.mRNAmiRNAinteractionnetworknodes..docx
- SupplementaryTableS4.MultivariateCOXregressionanalysistoPEMRGsassociatedwithOSinTCGALUAD..docx
- SupplementaryTableS13.ReverseTranscriptionReactionMix.xlsx
- SupplementaryTableS12.GenelevelprognosticanddiagnosticperformanceofthesixPEMsignaturegenesinTCGALUAD.docx
- SupplementaryTableS14.qPCRReactionMix.xlsx
- SupplementaryTableS16.RTqPCRPrimerSequences.xlsx
- SupplementaryTableS17.qPCRCyclingProgram.xlsx
- SupplementaryTableS11.ClinicopathologicalCharacteristicsofTCGALUADPatients.docx
- SupplementaryTableS18.BaselineclinicopathologicalcharacteristicsoftheRTqPCRcohort.docx
- SupplementaryTableS15.RTqPCRRawDatafor19PairedLUADSamples.xlsx
- SupplementaryFigureS1.docx